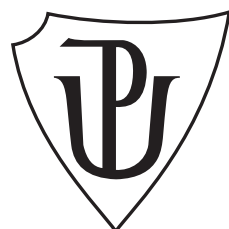


PALACKÝ UNIVERSITY OLOMOUC  
FACULTY OF SCIENCE  
JOINT LABORATORY OF OPTICS

**MASTER THESIS**

Characterization of semiconductor detectors  
for gamma-rays detection and their  
application in Mössbauer spectroscopy.



Author: **Daniel Staník**  
Study program: N0533A110002 Applied Physics  
Field of study: 1702T001 Applied Physics (AFYZ)  
Form of study: Full-time  
Supervisor: Mgr. Aleš Stejskal Ph.D.  
Deadline: May 2024

I would like to thank my supervisor Mgr. Aleš Stejskal Ph.D. for his support, guidance and feedback during the whole process of writing this thesis. I would also like to thank my former supervisor Mgr. Leo Schlattauer Ph.D. for the necessary support at the very beginning of the work on the experimental part of this thesis.

## **DECLARATION**

I hereby declare that I elaborated this bachelor thesis independently under the supervision of Mgr. Aleš Stejskal Ph.D., using only information sources referred in the Literature chapter.

In Olomouc April 28, 2024

.....  
Daniel Staník

# Bibliografická identifikace

Jméno a příjmení autora	Daniel Staník
Název práce	Charakterizace polovodičových detektorů pro detekci gama záření a jejich aplikace v Mössbauerově spektroskopii.
Typ práce	Diplomová
Pracoviště	Společná laboratoř optiky
Vedoucí práce	Mgr. Aleš Stejskal Ph.D.
Konzultant	Mgr. Leo Schlattauer Ph.D.
Rok obhajoby práce	2024
Abstrakt	Tato práce je věnována vývoji polovodičového detektoru pro nízkoenergetické gamma fotony. Popisuje testování PIN fotodiod, vývoj analogových elektornických obvodů pro gamma a Mössbauerovu spektroskopii a také se zabývá komparačními měřeními mezi polovodičovými detektory a jinými typy detektorů. PIN fotodioda, PCB, MS, gamma spektrum, předzesilovač
Klíčová slova	
Počet stran	65
Počet příloh	1
Jazyk	anglický

## Bibliographical identification

Autor's first name and surname	Daniel Staník
Title	Characterization of semiconductor detectors for gamma-rays detection and their applica- tion in Mössbauer spectroscopy.
Type of thesis	Master
Department	Joint Laboratory of Optics
Supervisor	Mgr. Aleš Stejskal Ph.D.
Consultant	Mgr. Leo Schlattauer Ph.D.
The year of presentation	2024
Abstract	This thesis is dedicated to the development of of semiconductor detectors for low en- ergy gamma photons. It describes the test- ing of PIN photodiodes, the development of analog electronic circuits for the pur- poses gamma and Mössbauer spectroscopy and also deals with comparative measure- ments between semiconductor detectors and other types of detectors.
Keywords	PIN photodiode, PCB, MS, gamma spec- trum, preamplifier
Number of pages	65
Number of appendices	1
Language	english

# Contents

<b>Introduction</b>	<b>8</b>
<b>1 Gamma rays properties and matter interaction</b>	<b>9</b>
1.1 Gamma emission . . . . .	9
1.2 Passage of radiation and particles through matter . . . . .	9
1.2.1 Gamma matter interaction . . . . .	10
1.2.2 Characteristic energy spectra . . . . .	12
<b>2 Gamma rays detection</b>	<b>14</b>
2.1 Properties and parameters of detectors . . . . .	14
2.1.1 Gas proportional detectors . . . . .	14
2.1.2 Scintillation detectors . . . . .	14
2.1.3 Detectors based on semiconductors . . . . .	15
<b>3 Semiconductor detectors with p-n junction</b>	<b>16</b>
3.1 The Structure of semiconductor . . . . .	16
3.1.1 Band structure . . . . .	16
3.1.2 Occupation of states . . . . .	17
3.1.3 Semiconductor Crystals . . . . .	17
3.1.4 Direct and indirect semiconductors . . . . .	17
3.2 The p-n junction . . . . .	17
3.3 Detection mechanism . . . . .	18
3.4 Main noise sources and resolution limitations . . . . .	19
3.4.1 Fano noise . . . . .	19
3.4.2 Thermal noise . . . . .	20
3.4.3 Recombination and trapping . . . . .	20
3.5 Structure and parameters of Si PIN detector . . . . .	20
3.6 Available Si PIN detectors . . . . .	21
3.6.1 Hamamatsu S14605 . . . . .	22
3.6.2 BPW34 . . . . .	22
3.6.3 OPF430 . . . . .	23
<b>4 Mössbauer effect and spectroscopy</b>	<b>24</b>
4.1 Physical concept . . . . .	24
4.1.1 Resonance emission and absorption . . . . .	24
4.1.2 Interaction of nuclei with local fields . . . . .	25
4.2 Mössbauer spectroscopy . . . . .	25
4.3 $^{57}\text{Fe}$ spectroscopy . . . . .	26
4.4 MS spectra quality parameters . . . . .	29

<b>5 Electronics for signal readout and analysis</b>	<b>30</b>
5.1 PIN detector connection and support electronics . . . . .	30
5.1.1 Voltage source . . . . .	30
5.1.2 Shielding and grounding . . . . .	31
5.1.3 Cooling . . . . .	31
5.2 Spectrometric chain . . . . .	31
5.2.1 Pre-amplification . . . . .	32
5.2.2 Shaping . . . . .	35
5.2.3 Multichannel analysis (MCA) . . . . .	35
<b>6 Gamma spectrum software analysis</b>	<b>37</b>
6.1 Peak searching procedure . . . . .	37
<b>7 Gamma detection testing</b>	<b>39</b>
7.1 Noise and its reduction . . . . .	41
7.1.1 Electromagnetic noise reduction . . . . .	41
7.1.2 Thermal noise reduction . . . . .	42
7.2 Detection test of the $^{57}\text{Co}$ spectra . . . . .	43
7.2.1 S14605 test . . . . .	44
7.2.2 BPW34 test . . . . .	44
7.2.3 OPF430 test . . . . .	45
<b>8 Design of integrated amplifier</b>	<b>47</b>
8.1 Scheme and layout . . . . .	47
8.2 Grounding and Shielding . . . . .	52
8.3 Photodiode input and preamplifier . . . . .	52
8.4 Amplification . . . . .	52
8.5 Voltage supply . . . . .	52
<b>9 <math>^{57}\text{Co}</math> spectra measurement with integrated amplifier</b>	<b>54</b>
9.1 Measurement setup . . . . .	54
9.2 Si PIN detector measurement . . . . .	56
9.3 Scintillator and gas detector measurement . . . . .	57
9.4 Results . . . . .	58
<b>10 Mössbauer spectra measurement</b>	<b>60</b>
<b>Conclusion</b>	<b>63</b>

# Introduction

In nuclear and particle physics, semiconductor-based detectors are becoming increasingly common due to the many unique properties they offer. Semiconductor detectors have a very wide range of applications, from spectroscopy to large particle experiments such as ATLAS at CERN.

This thesis is dedicated to the development of a semiconductor detector based on a Si photodiode for the detection of low energy gamma photons. The detection of low-energy gamma photons plays a crucial role in the field of Mössbauer spectroscopy, which requires a detector with sufficient detection efficiency and energy resolution.

The first four chapters are theoretical and provide a brief introduction to the mechanisms of gamma photon interaction and detection, the properties of semiconductor detectors and the basics of Mössbauer spectroscopy. These chapters are followed by a chapter describing the specifications of nuclear instruments used to build a spectrometric chain, and then a chapter introducing the numerical analysis of gamma energy spectra.

The experimental part begins with the gamma detection tests of selected photodiodes and is followed by a chapter filled with the technical description of the PCB integration of the spectrometric chain. The thesis ends with two chapters presenting the results of gamma energy spectra and Mössbauer spectra measurements.

# Chapter 1

## Gamma rays properties and matter interaction

### 1.1 Gamma emission

Gamma rays are high-energetic photons, but the major difference to the X-Ray photons is that they originate only from atomic nucleus upon its deexcitation from higher energy level to lower. The energy levels of nucleus are similar to the levels in electron shell - discrete, characteristic for every isotope and can be described by quantum numbers. The gamma emission usually follows alpha or beta decays. The gamma photon is emitted due to the fact, that the new nucleus is created in an excited state.

### 1.2 Passage of radiation and particles through matter

Interaction of a particle (radiation) with another particle (atom, nuclei, free electron) or with continuous matter can result into many types of interactions and effects - scattering of a particle from incident direction, creation of new particles and nuclei, annihilation of incident particle etc. It mainly depends on particle's energy, electric charge, spin and mass, but also on the properties of target particle or matter. The physical quantity describing the probability of a specific interaction of particle with single point target is known as the cross section. Normalized to the unit solid angle - differential cross section:

$$\frac{d\sigma}{d\Omega} = \frac{1}{F} \frac{dN_s}{d\Omega} \quad (1.1)$$

Where  $F$  is a particle flux,  $\Omega$  is a solid angle and  $N_s$  is the average number of scattered particles per unit time. And the total cross section is given by integration:

$$\sigma = \int \frac{d\sigma}{d\Omega} d\Omega \quad (1.2)$$

However, to characterize the interaction probability of particle with continuous matter, which contains many interaction centres (defined by their density), other assumptions have to be made. The average number of scattered particles is given by:

$$N(\Omega) = F A N \delta x \frac{d\sigma}{d\Omega} \quad (1.3)$$

and integrated over the entire solid angle:

$$N_{tot} = FAN\sigma\delta x \quad (1.4)$$

The  $A$  is a total area perpendicular to the flux,  $\delta x$  is the material thickness and  $N$  is the density of interaction centres.

Heavy charged particles (such as alpha particles, protons, muons, pions) lose their energy mainly due to the atomic electrons collisions. Due to their mass which is much higher than the mass of electrons ( $M \gg m_e$ ) they collide with, the direction of their path is left unchanged. The losses of energy per unit path is defined as stopping power  $\frac{dE}{dx}$ . The stopping power for the heavy charged particles is given by Bethe-Bloch formula which relates stopping power and particle's energy. However the Bethe-Bloch formula doesn't apply on low energies (Lindhard-Sharf nuclear loses) and on higher energies (bremsstrahlung radiation). The change of their path direction is possible by the second process with lesser probability - by the elastic scattering from nuclei.

Electrons and positrons have much smaller mass than the heavy charged particles, and thus the direction of their path is changed due to the movement in an electric field of nucleus. The bremsstrahlung radiation losses are mayor yet at low energies. However, the energy lost due to the collisions also comes to play - it is guided by special Bethe-Bloch formula, which takes the path direction change into account.

Other interaction effects are also possible (Cherenkov radiation emission, nuclear reactions), but they are rare or does not affect the particle's energy as those previously mentioned.

The interaction of neutrons is totally different due to the lack of charge.

The interaction effects for gamma rays are described more detail in the following chapter.

### 1.2.1 Gamma matter interaction

Due to the fact, that the gamma rays are photons, the gradual losses of kinetic energy inside materials (characteristic for the charged particles) are not observed. Instead the main observed effect is the attenuation of intensity of photon flux with the increasing thickness of the absorber material.

Three major interaction effects of gamma photons and matter are: Photoelectric effect, Compton scattering and Pair production. The cross section of these effect vary with gamma photon energy, with material and its density - high dependence on atomic number  $Z$ . There are also possible nuclear reaction such as the Mössbauer effect, but their observation requires very special conditions to be met.

The attenuation of photon flux has a form of exponential decay:

$$I = I_0 \exp(-\mu x) \quad (1.5)$$

where  $I_0$  and  $I$  are the radiation intensities and the parameter  $\mu$  is the total absorption coefficient, which describes the probability of interaction per unit length and is bounded with total cross section of single atom  $\sigma$  (combination of cross section of three main effects) by relation:

$$\mu = N\sigma = \sigma(N_a\rho/A) \quad (1.6)$$

where  $N$  - density of atoms,  $N_a$  - Avogadro number,  $\rho$  - material density and  $A$  - molecular weight.

The dependence of total cross section combined of the three main effect for lead on photon energy can be seen on fig. 1.1.

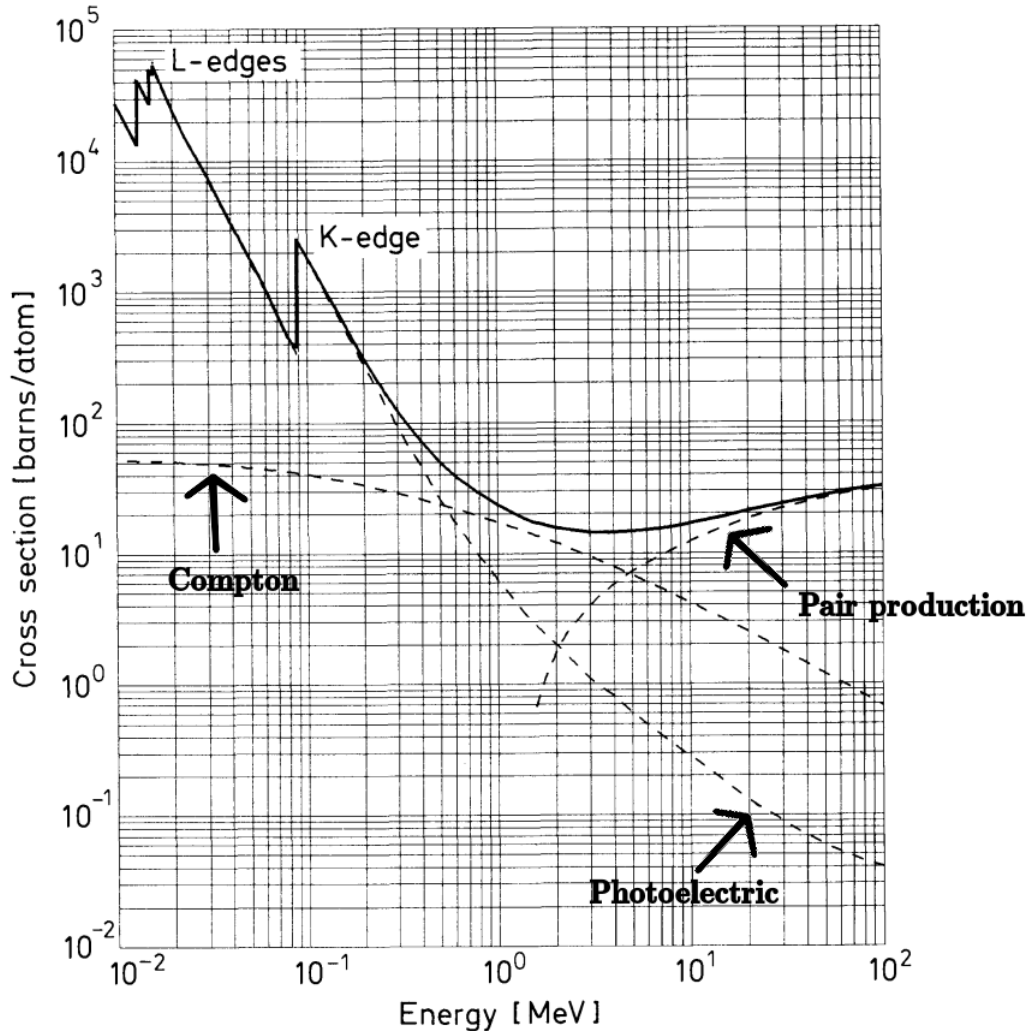


Figure 1.1: Example of total absorption cross section for high-energy photons for lead. Taken and modified from [4].

### Photoelectric effect

The photon is absorbed by electron from atomic shell. The electron is ejected and acquires the kinetic energy given by well-known equation:

$$E = hf - E_b, \quad (1.7)$$

where  $f$  is the photon frequency and  $E_b$  is the binding energy.

The Photoelectric effect can be observed only on electron bounded in atomic shell, due to the fact, that the nuclei can absorb the photon's momentum. The cross section usually falls with energy and can have characteristic peaks from K,L,M transitions. Two types of photoelectric effect can be distinguished - external and internal. External photoelectric effect results into ejecting the electron outside of the material - effect observed on photo cathodes. Internal photoelectric effect results into exciting the electron into the higher energy levels - in semiconductor it means from the valence band to the conduction band.

The photoelectric effect plays a key role when it comes to the detection of gamma photons.

## Compton scattering

Compton scattering is an effect, which is mainly observed on free electrons. It needs to be said, that the electrons in material are usually bounded, however, if the photon energy is much higher than the binding energy, the electron can be considered as free.

This effect causes, that the photon loses only a part of its energy and changes its direction. The energy is transferred to an electron accordingly to the laws of energy and momentum conservation and can be described by following relation:

$$E_e = E_1 - E_2 = E_1 \left( 1 - \frac{1}{1 + \frac{E_1}{m_e c^2} (1 - \cos \theta)} \right) \quad (1.8)$$

Where  $E_e$  - energy transferred to an electron,  $E_1$  - initial photon energy,  $E_2$  - scattered photon energy,  $m_e$  - the electron mass and  $\theta$  - angle of scattering. This equation can be used to calculate the positions of Compton edges in energy spectra by plugging the angle of maximum energy transfer ( $\theta = 180^\circ$ ).

## Pair production

At much higher energies, the photon can be converted into electron-positron pair. This effect happens near the nucleus, which absorbs a part of the original photon momentum.

The pair production along with electron bremsstrahlung radiation are key effects for electron-photon shower development. If the created electron/positron has sufficient energy, it emits bremsstrahlung photons. These bremsstrahlung photons can again interact via the pair production, and thus creating new electrons again. This process of shower development continues until the energy of electron/positron pairs drops under the energy, which is required to produce bremsstrahlung radiation. At lower energies, the electrons lose more of their energy by the atomic collisions rather than by bremsstrahlung.

Negative effects arising from this type of interaction like creation of single and double escape peaks or annihilation peaks in spectra will not be observed, because for low-energy gammas the cross-section is very small. That means that for the purposes of this thesis, this interaction effect could be neglected.

### 1.2.2 Characteristic energy spectra

Every gamma source emits its characteristic photons with certain probabilities. However, before these photons are captured by detector, many effects can occur in environment or inside the detector - photons can interact various materials without detection purpose such as shielding, spectrum can be altered by noise events in detector etc.

Inside detector the low-energy spectra can be affected by:

- X-ray escape peaks - If the photo-effect occurs on atomic energy levels, the characteristic X-ray of the detector material is emitted. The escape peak has the energy of captured photon minus the energy of escaped gamma ray.
- Compton continuum with edge - the photon interacts inside detector by Compton scattering, scattered photon leaves the detector.

In environment the low-energy spectra can be affected by:

- Characteristic X-rays - radiation induced fluorescence usually from the shielding material (Pb).
- Backscatter peak - Compton scattering which occurred over a large angle.

For Mössbauer spectroscopy the  $^{57}\text{Co}$  is usually used with gamma spectra shown below:

# Chapter 2

## Gamma rays detection

### 2.1 Properties and parameters of detectors

The main parameters which are crucial for purposes of Mössbauer are detection efficiency and energy resolution at low gamma energies.

Nowadays three main types of detectors are employed on the field of nuclear physics - gas, scintillation and semiconductor. The Mössbauer spectrometer setups in laboratories of Department of Experimental Physics of Palacky University are usually based on gas or scintillation detectors.

#### 2.1.1 Gas proportional detectors

The gas detectors are usually tubes with two electrodes filled with a special gas mixture. The incoming particle ionizes the gas, creating free ions and electrons. Gaseous detectors are operated in proportional regime, which is characterized by proportional amplification of charge carriers. The advantage of gaseous detectors is that they offer good energy resolution, but on the other hand their detection efficiency is low mainly due to the fact, that the gas density is small. Count rates are also affected by the long duration of the ionization effect. For operation they require high voltages (usually over 1000 V) and in case of flow counters they also require pressure cylinders.

#### 2.1.2 Scintillation detectors

By scintillation detector is usually meant a scintillation crystal coupled with a photomultiplier tube (PMT). The first conversion of the photon energy happens inside the scintillation crystal, where the incoming particle generates number of photons linearly dependent on its energy. These photons are captured by PMT's photo-cathode, where they are converted into electrons, and then multiplied on PMT's dynodes. This amplification requires high voltages (starting from 500 V). The internal amplification inside PMT can be around  $10^6$ .

The detection efficiency is very high and due to the short duration of excitation process, they can be used at high count rates.

However, their energy resolution is much worse than in case of gases and semiconductors. The gamma spectra obtained this way usually have distorted wide peaks, which negatively affects Mössbauer spectrometry - decreases SNR. Also the employment of PMTs inside the magnetic fields is very problematic and requires a difficult instrumentation.

### 2.1.3 Detectors based on semiconductors

The semiconductors offer the best energy resolution - the energy required to create a charge carrier is usually very small (in order of eVs). The detection efficiency is a function of gamma photon's energy and detector thickness. The efficiency can be very high - for example some Si PIN diodes have their efficiency near 100 % up to 10 keV [11].

However, semiconductors are usually more expensive than the other types of detectors. They can be used as direct radiation detectors (more often) or there is also a possibility to couple them with a scintillator crystal.

One problem with semiconductor detector is that there is no internal amplification, so the signals coming out of the detectors have to be strongly amplified by electronics. However, they are small and compact. They also don't require high voltage sources or heavy pressure cylinders to operate. These facts are crucial if it comes to making more compact Mössbauer spectrometers - for example MIMOS II [27] based on 4 Si PIN diodes was a part of two rovers Spirit and Opportunity on their mission on Mars.

# Chapter 3

## Semiconductor detectors with p-n junction

The semiconductor structures has unique properties, which make them usable not only for a particle/photon detection. There are many types of semiconductor detectors - conventional detectors of light intensity with spectral range from infrared to UV - photoresistors and photodiodes, low intensities and single photons detectors - avalanche photodiodes (APDs), for imagining - CCD and CMOS cameras, x-ray, gamma and other particles rates and energy detectors - special photodiodes, for particle position and energy measurements - matrix drift and strip detectors. The essential role for gamma spectroscopy have the p-n junction detectors.

To detect Mössbauer 14.4 keV gammas our primary choice are the Si PIN diodes for direct detection due to the high detection efficiency under 25 keV [11].

### 3.1 The Structure of semiconductor

Since we are not dealing with single atoms characterized by the well-known discrete energy levels, but with solid crystals, there is another model describing the energy levels - the band structure. The energy levels are very close each other that they nearly form a continuum. This different behaviour is a result of a periodical potential inside the crystal lattice. However, the electron energy  $E_n$  is not the only quantum number describing the behaviour of electrons inside the periodical potential. By solving Schrödinger equation with the help of so-called Bloch's theorem, we come to a conclusion that the second important quantum number is the wave vector  $\mathbf{k}$ . These two quantum numbers are bounded together by dispersion relations  $E = E(\mathbf{k})$ , which is characteristic for every crystal and may play role when it comes to transitions of electrons between bands.

#### 3.1.1 Band structure

The basic difference between conductors, insulators and semiconductors is the valence and conduction band structure. In case of conductors, the valence band overlaps the conduction band. The electrons in conduction band can move nearly freely throughout the crystal. For insulators, there is no overlap, and the energy band gap  $E_g$  between the two bands is so high, that it makes any transitions of electrons nearly impossible. However in case of semiconductors, the  $E_g$  is small enough to allow the electron jump into the conduction band and leaving the hole in valence band after receiving a sufficient

amount of energy - in form of thermal energy  $E_T = kT$ , energy in static electric field  $E_s = -e\phi$  or as a photon with energy quantum  $E_{\text{photon}} = \hbar\omega$ . The last one is the most important, because it allows us to use the semiconductors as detectors. Both the electron and hole participates on conduction, but they have to be treated as quasiparticles with their specific masses and mobilities.

### 3.1.2 Occupation of states

The occupation probability of states in band structure is given by Fermi-Dirac distribution since the electrons are the Fermions with the exclusion rules.

The possible occupied state where occupation probability drops below 50 % is called the Fermi level with Fermi energy  $E_F$ . For ideal pure semiconductor at  $T = 0$  K, the  $E_F$  lies in the middle of the band gap. With increasing temperature, in most materials the Fermi-level moves upper towards the conduction band.

### 3.1.3 Semiconductor Crystals

The semiconductor materials have usually form of a crystal of diamond structure (two FCC lattices bounded together.) with the lattice atoms bounded by a covalent bond. However in real crystals there are also defects and impurities which may alter the functionality. The impurities can be added on purpose to enhance the properties we seek in procedure called doping.

The suitable materials for construction of ionizing radiation detectors are Ge - very good energy resolution, requires cooling, Si - great efficiency under 25 keV, easier fabrication since many other semiconductor devices are being made of Si and CdTe - used in wide-spectre X-Ray and Gamma Ray Detectors.

The fabrication of semiconductors for purposes of detection includes many complicated processes, because the detector requirements on crystal purity are very high.

### 3.1.4 Direct and indirect semiconductors

The shape of dispersion relations  $E(\mathbf{k})$  divides the semiconductors into two categories - direct and indirect semiconductors. For direct semiconductors the minimum in conduction band and maximum in valence band have the same  $\mathbf{k}$ , so the transition can occur after the  $E_g$  is supplied. In case of indirect the minimum and maximum have different  $\mathbf{k}$ . To make transition, additional momentum has to be served (for example by phonons) or the supplied energy must be much larger to allow transition to the higher state. The Si crystal is an indirect semiconductor.

## 3.2 The p–n junction

The intrinsic semiconductors have only a little field of applications. We can alter the behaviour by adding a specific impurities and create an extrinsic semiconductor. The Si atom has 4 valence electron which form a covalent bond with other Si atoms. If Si atom is replaced with atom with 5 valence electrons, one of them will have a very weak bond. By doping the intrinsic semiconductor with these atoms we create the *n*-type with additional electrons, which are nearly localized in conduction band. However, the crystal as whole stays neutral. Similar way doping by atoms with only 3 valence electrons, there will be holes in valence band, which can participate on conduction -

the *p*-type. In band structure These atoms create energy levels in band structure, but in room temperatures, they are all mostly ionized and participate on conduction. The full theoretical treatment of doping is very complex, considers many other quantum and statistical physics aspects, and have no use for the purposes of this thesis.

The special effects will arise when *p*-type and *n*-type are bound together. The holes from *p*-type and electrons from *n*-type will start to diffuse to the other region. However, this movement alter the charge density, which leads to creation of built-in voltage which in the end cancels the diffusion. This creates the depleted region, where are no free charge carriers.

Another theoretical view is that the electrons will rearrange, because the Fermi-level has to be same throughout the crystal, while the Fermi-level for stand-alone *p*-type is nearer to the valence band and for *n*-type is nearer to the conduction band. The potential created this way equalizes the different Fermi levels.

The p-n junction can be connected to source voltage in two ways. The *p* layer on plus - the source voltage (refereed as bias) reduces the size of depleted layer until it completely vanishes (bias goes against built-in voltage) and the p-n junction becomes conductive - forward direction or in reverse direction - *p* layer on minus (bias goes with built-in voltage), the size of depletion layer increases.

The p-n junction has many unique properties, which are commonly used in form of classical diodes. However, it is also crucial for the detection since the free charge carriers (if somehow created) in depleted layer are pushed towards electrodes by electric field and form a photocurrent.

For the purposes of design in electronic circuits, the detectors are usually modelled as classical p-n diodes, which are connected to the source of the bias voltage in reverse direction. In case of detection, the detector can be also modelled as a current source.

The voltage across the depleted layer could be modelled as a simple plate capacitor. The capacitance of p-n junction plays a significant role - it alters the dynamical parameters of the detection circuits - it can alter the rising edges of pulses, alter the entire frequency spectra, increase/decrease the SNR. By varying the source voltage we vary this capacitance too.

### 3.3 Detection mechanism

If we want to detect a particle or photon, is has to interact with the detector material - in semiconductor the creation of electron-hole pairs is observed. This could be achieved by interaction mechanisms described in previous chapters, which differ for every type of particle and energy. In case of low-energy gamma the two main mechanisms which take place in producing the charge carriers are photo-effect (internal) and Compton scattering.

The main of purpose of semiconductor as a detector, is to perform a linear conversion of the particle/photon energy into the free charge carriers - electrons in conduction band and holes in valence band. The average energy needed to create a single electron-hole pair is usually a fix constant - in Si it is  $\epsilon = 3.6 \text{ eV}$  [6]. Since the Si is an indirect semiconductor, this value is not equal to gap energy, which is lower ( $E_g = 1.12 \text{ eV}$ ).

The gamma photon striking the detector firstly interacts with a single electron. If the photo-effect takes its place, the primary electron with energy much higher than the thermal excitation will ionize the electrons from all over the valence band pushing them into higher states from conduction band. These Electrons in conduction band de-excite themselves into lower states of conduction band and the holes redistribute themselves

to the upper states in valence band. This de-excitation process releases energy again and that leads to the cascade of further excitations and interactions, which produce many electron-hole pairs - the charge cloud. Number of generated electron-hole pairs  $n$  is simply given by relation:

$$n = \frac{E_{\text{gamma}}}{\epsilon}. \quad (3.1)$$

In case of Compton scattering, the scattered photon may escape the detector without any other interaction taking the rest of its energy out of the detector. This results into energy distortion. The Compton without any other interaction (Compton again or photoeffect) is typical for thin detectors since there is insufficient thickness to stop the scattered photon again. In detected gamma energy spectrum this leads into the Compton continuum with the compton edge, which devalues the spectra.

An ideal very thick detector could solve this problem, because every possible interaction and all the following sub-interactions will happen inside the detector and will result into electron-hole generation. The detector of this kind would have only the full energy peaks without any other unwanted counts. However, construction of such detector is impossible due to the many technical and manufacturing problems arising with increasing dimensions.

In case of p-n junction the created charge carriers in depleted layer are pushed towards electrodes by internal electric field. The electronics accumulates the charge and converts it into the voltage pulse signal, which is then analysed to extract the energy information. Since the depleted layer is the only part where the detection can occur, its obvious that for detector purposes it should be large as possible.

To achieve the greater dimensions of the detection part, the p-n junction can be upgraded to p-i-n junction, which contain additional intrinsic layer between  $p$  and  $n$  part, which work as fix size depleted layer. The detectors with p-i-n junction are referred as PIN diodes. The additional intrinsic layer also decreases the capacitance and increases the time needed for charge carriers to exit the detection part.

## 3.4 Main noise sources and resolution limitations

The detection efficiency and the energy resolution are strongly dependent on noise which alters the signal. While some negative effects are caused by outer conditions such as temperature or by noise in electronics, some originate strictly from semiconductor material properties and only chance to minimize them is during the crystal's preparation.

### 3.4.1 Fano noise

The physical effect inside the semiconductor itself which limits the measured energy resolution is the fact that not all of the particle's energy is transformed into charge carriers. Some fraction of energy can be consumed to induce lattice vibrations (phonons). Statistically the relative resolution can be described by following equation:

$$\frac{\Delta E}{E} = 2.35 \sqrt{\frac{F\epsilon}{E}}, \quad (3.2)$$

where  $E$  is incoming particle's energy,  $\epsilon$  is the average energy needed for the single pair creation and  $F$  is a Fano Factor. Fano Factor is a special statistical constant which

describes the dispersion in counting process. For Poisson distribution the  $F$  is 1. If we consider the case of 14.4 keV gamma inside Si ( $\epsilon = 3.6$  eV,  $F = 0.12$ ), the  $\frac{\Delta E}{E}$  is equal to 1.3 % and  $\Delta E$  is 185.4 eV.

This resolution is sometimes called intrinsic, because the real resolution is much worse. This model does not consider other sources of noise coming from the amplification in electronics, dark currents e.g.

### 3.4.2 Thermal noise

It was mentioned that the electrons can be also excited by thermal fluctuations. However, since the many of detector's materials are indirect semiconductors, the thermal excitations are carried through the intermediate states inside the band gap. These states have the origin in imperfections and impurities inside the crystal lattice. The electrons and holes generated this way can join the charge cloud generated by detected particle and decrease the SNR. This phenomenon is usually called dark current.

The thermal fluctuations are much more significant for materials which require less energy to excite the electrons to the conduction band such as Ge. These detectors always have to be operated at low temperatures. Even the room temperature can lead up to the breakdown and destruction of a detector. For Si, the valence and conduction band are more distant. so the thermal fluctuations are not so critical. However, the applied bias voltage in reverse direction also increases the dark current.

### 3.4.3 Recombination and trapping

The effect which goes against the successful collection of charge carriers and thus affects the detection efficiency and the energy resolution is recombination. In pure crystals, the electron can recombine with hole only when they have the same  $\mathbf{k}$ . However, inside real crystals there exists impurities, which allow carriers to recombine - recombination centres. The charge collection must take much less time than it takes the carriers to recombine.

Another effect caused by the very same impurities is trapping. The trapping centres capture electron or hole and release it after certain time. This effect alter the signal pulses and can decrease maximum possible counting rate.

Energy levels near the centre of band gap are primary responsible for recombination and trapping, which means that the impurities causing this are not the impurities which were added in doping, because these have their additional energy levels near the bands.

## 3.5 Structure and parameters of Si PIN detector

One of the most important parameter is the size of the photosensitive area, which has to be large as possible for effective collection of radiation. This area has to be treated with extreme caution since every damage, adsorption of impurities or dew condensation due to the high environmental humidity reduces the active photosensitive area.

Its obvious that for the interactions inside the detector the most crucial layer dimensions are those, which are parallel to the direction of incident radiation - the thicknesses of P and I regions. The dead region (P) has to be thin as possible to reduce probability that the particle interacts in place where the generated charge cloud would nearly immediately recombine. The active depleted (I) layer has to be thick enough to make

all the interactions happen inside itself. The schematic of PIN diode can be seen on fig. 3.1.

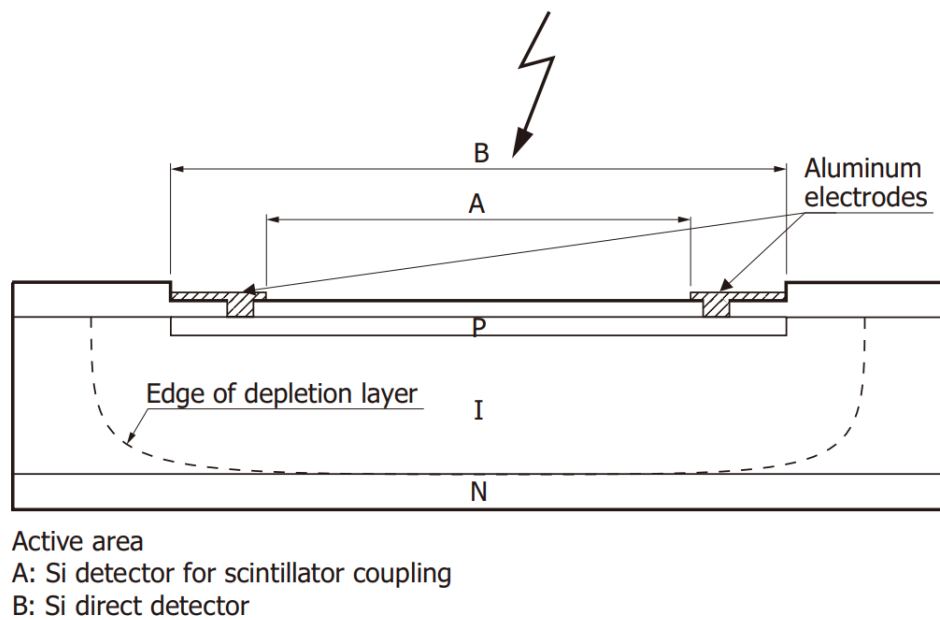


Figure 3.1: Cross section of Si detector for scintillator coupling and Si direct detector [18].

### 3.6 Available Si PIN detectors

For testing we have chosen one professional Hamamatsu S14605 PIN diode and two commercial PIN diodes: BPW34 - visible and near infrared radiation detector, OPF430 - originally designed to be used in optical fibres.

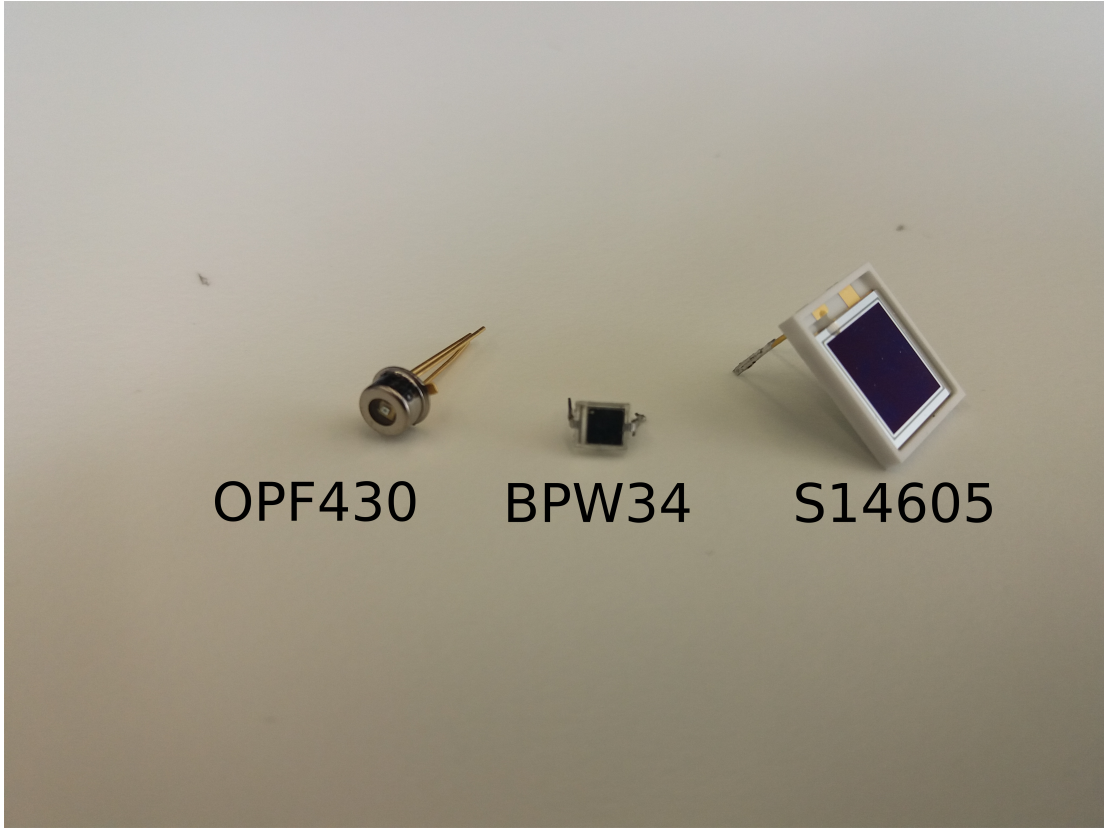


Figure 3.2: PIN diodes - OPF430, BPW34 and S14605.

### 3.6.1 Hamamatsu S14605

The professional S14605 is designed to be used as a direct radiation detector. It offers a very large photosensitive area and a low capacitance.

Parameters [17]:

- Maximum reverse voltage  $U_R$ : 150 V
- Photosensitive area: 81 mm<sup>2</sup>
- Capacitance: 25 pF at  $U_R = 100$  V
- Dark current: 8 nA at  $U_R = 100$  V
- Depletion layer: 0.5 mm
- Cost: 5000 CZK

### 3.6.2 BPW34

BPW34 is a very low cost radiation detector. There were manuals [14] how to use BPW34 as a beta particle detector, and since it is a Si PIN diode, it worths a try and test it for our gamma detection purposes.

Parameters [33]:

- Maximum reverse voltage  $U_R$ : 32 V
- Photosensitive area: 7.5 mm<sup>2</sup>

- Capacitance: 25 pF at  $U_R = 3$  V
- Dark current: 2 nA at  $U_R = 10$  V
- Depletion layer: not specified
- Cost: 11 CZK

### 3.6.3 OPF430

OPF430 is originally meant to be a low-cost detector for fiber optic applications. However, there were publications [5], which described the possibility of using similar diode OPF420 in low-energy gamma spectroscopic chains as a low-cost detector.

Parameters [15]:

- Maximum reverse voltage  $U_R$ : 100 V
- Photosensitive area: not specified, smaller than BPW34
- Capacitance: 1.5 pF at  $U_R = 5$  V
- Dark current: 0.1 nA at  $U_R = 5$  V
- Depletion layer: not specified
- Cost: 340 CZK

# Chapter 4

## Mössbauer effect and spectroscopy

Mössbauer effect is an interaction, which can under certain circumstances occur on atomic nuclei. It is recoilless resonance emission/absorption of gamma photons by nuclei of source/absorber with discrete nuclear energy levels. This effect has a special application in the field of material research - the Mössbauer spectroscopy (MS), which is a nuclear experimental technique and a special type of gamma spectroscopy, which uses the appropriate nuclei in studied sample as probes of local electric and magnetic fields.

This technique is capable of providing many unique information in material research, geology, chemistry and biology - study of phase and chemical composition of solid materials, study of local magnetic fields and spin states and in-situ measurements of phase transitions. The main disadvantage of this technique is the fact that there is not an appropriate radiation source for many isotopes. The major significance has iron and its isotope  $^{57}\text{Fe}$  with radiation source  $^{57}\text{Co}$  (which decays into an excited state of  $^{57}\text{Fe}$  with half-life 271.81 days [13]), which allows the Mössbauer spectroscopy to be employed in many fields investigating iron compounds

### 4.1 Physical concept

#### 4.1.1 Resonance emission and absorption

In previous chapters was mentioned, that the atomic nuclei are quantum systems with discrete energy levels (analogous to the energy levels of electron shell), thus upon deexcitation or excitation they emit/absorb gamma photon with energy  $E_0$  equal to the difference between the levels. For the free, stationary nucleus, the emitted/absorbed energy spectra follow the shape of Lorentzian curve.

However, these emitted/absorbed energy spectra may be altered - due to the momentum conservation law, part of the gamma photon energy is transferred to the kinetic energy of nucleus, crystal as whole body or is transformed into lattice vibrations (phonons). In the case of free, stationary nuclei, momentum and energy transfers are so high, that the emission and absorption spectra are shifted to different directions by large energetic values, which makes the resonance absorption impossible to observe. However, the nucleus bounded into the crystal lattice is a different case - the crystal as whole body will absorb the momentum. If we consider, that the entire crystal has much larger mass than the nucleus, the energy transfer into crystal's kinetic energy will be very small - the gamma photon energy remains nearly unaltered and that results into recoilless emission/absorption. In this case the emission and absorption energy spectra

have overlap and that makes the resonance absorption (Mössbauer effect) observable [8].

#### 4.1.2 Interaction of nuclei with local fields

The nucleus bound inside the lattice surrounded by electrons arranged according to the chemical bonds has perturbed energy levels, which is due to the interaction of nucleus with local electric and magnetic fields, resulting in each phase or chemical composition has its own nuclear emission/absorption spectrum - Mössbauer spectrum. The quantum physics has very-well known computation techniques to describe these variations in energy spectra - the perturbation theory.

The main properties of nucleus which induces the interactions with local electric and magnetic fields are: atomic number  $Z$ , quadrupole momentum  $Q$  and its spin  $I$  along with its projections. For spectroscopy there are three main hyperfine interaction [8]:

- Electric monopole interaction - the interaction between the protons of nucleus and the s-electrons (which have non-zero probability of being found inside nucleus). It results into isomer shift of energy levels  $\delta = E_M - E_0$ . The  $\delta$  has to be defined with respect to some fixed energy level, for example to the level of the used source. This type of MS spectra is usually referred as a singlet.
- Electric quadrupole interaction - the inhomogeneous electric field inside nucleus interacts the quadrupole momentum  $Q$  of the nuclei. It results into energy variations with respect to the square of magnetic quantum number  $E_Q \sim m^2$ - the states which allows different values of  $|m|$  are splitted into sub-states.
- Magnetic dipole interaction - the spin  $I$  is tied up with magnetic momentum via relation  $\mu = \gamma I$ , where  $\gamma$  is a gyromagnetic ratio. This magnetic momentum interacts with magnetic fields inside nucleus and results into nuclear Zeeman effects - the splitting of the states with respect to possible values of magnetic quantum number  $m$ . The main difference from the quadrupole interaction is that the spin orientation also matters. The magnetic dipole interaction has a significant role when it comes to study the magnetic properties of materials.

Each of these effects can occur separately or simultaneously with the others.

## 4.2 Mössbauer spectroscopy

To obtain the spectra, we can use one of the several measurement setups with given geometries. In laboratories there are dominant the setups employing transmission or backscattering geometry with sample as an absorber and with the doppler modulation of the gamma photons energy. The transmitted photons or other products developed upon deexcitation are detected by appropriate detector with electronics to accumulate the Mössbauer spectra. The source is attached to the doppler modulator (transducer), and by the relative velocity of source and absorber the energy of gamma photons is modulated typically in the range of about  $\pm 1 \mu\text{eV}$ .

For transmission geometry the key concept of measurement is that if we irradiate the sample placed as an absorber by gamma spectrum generated by the doppler modulator, the gamma photons with energy equal to one of the transitions (resonant energies) are

absorbed with certain probability. The detector is situated behind the absorber and measures the number of gamma counts at defined energy step. The minimal counts are measured around the resonant energy. The transmission geometry Mössbauer spectra can be seen on picture ??.

The concept of backscattering geometry is similar in many ways, but the main difference is the detection of the secondary particles. The nuclei in the sample are excited by appropriate gamma photons and in short time, they decay back into the original state with some effects following - reemission of the "original" gamma photons in random direction, emission of electrons from the shell (ejected by deexcitation energy quanta, also called conversion electrons) followed by characteristic x-rays or possibly by auger electrons. The detection of electrons and x-rays instead of gamma photons have many advantages and disadvantages and for certain application, the usage of backscattering geometry could be more appropriate. For example, the detection of conversion electrons could handle the surface characterization of the sample due to the lower transmittance of electrons when compared to gamma photons.

There are also different configurations - irradiation by synchrotron radiation (which can produce continuous energy spectra with high iluminance), using the sample as an source etc.

### 4.3 $^{57}\text{Fe}$ spectroscopy

One of the isotopes, on which we are capable to observe a Mössbauer effect is  $^{57}\text{Fe}$  (relative abundance only 2.21% [28]). As a source is used  $^{57}\text{Co}$ , which decays into second excited state of  $^{57}\text{Fe}$  by electron capture. The new  $^{57}\text{Fe}$  nuclei can deexcite itself by two ways (see fig. 4.1) - by direct deexcitation onto the ground state by emission of 136.5 keV photon or by deexcitation onto the first excited state by emission of 122.1 keV photon. This first excited state is essential since its used to study the hyperfine interactions. After the lifetime of the first excited state the 14.4 keV photon is emitted (or other possible conversion products) when falling into the ground state. The  $^{57}\text{Fe}$  spectroscopy in transmission geometry is based on detection of the 14.4 keV gamma photons. This thesis is mainly devoted to the application of semiconductor detectors for the detection of these 14.4 keV gamma photons. The  $^{57}\text{Fe}$  spectroscopy can also be performed in backscattering geometry by the detection of the conversion electrons or conversion x-rays with energies around 6.4 keV.

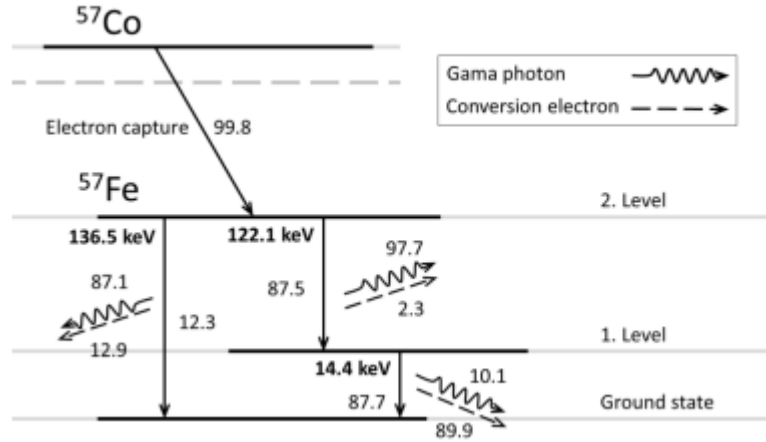


Figure 4.1: Decay scheme of  $^{57}\text{Co}$ , taken from [1].

The entire spectrometric setup consist of several parts:

- Source of 14.4 keV gamma -  $^{57}\text{Co}$  radioactive nuclei built-in crystal lattice (mostly in a rhodium matrice). The source is attached to the transducer.
- Transducer for doppler modulation. It mostly consists of two coils surrounded by permanent magnets - one for driving the Doppler energy modulation and second for the velocity measurement. The system is driven by PID (proportional integral derivative) or MPC (model predictive control) controller for precise velocity and energy control. The velocity can be either constant or with constant acceleration.
- detector of transmitted/backscattered gamma radiation, conversion electrons or x-ray along with readout and evaluation electronics including amplifiers, singlechannel or multichannel analysers etc. It is also necessary to consider, that the already mentioned conventional detectors have not sufficient energy resolution to distinguish the energy of perturbed states. Because of that, the count rates are synchronised with the velocity signal (actual modulated energy of the source), which is used to address the channels for spectra accumulation.

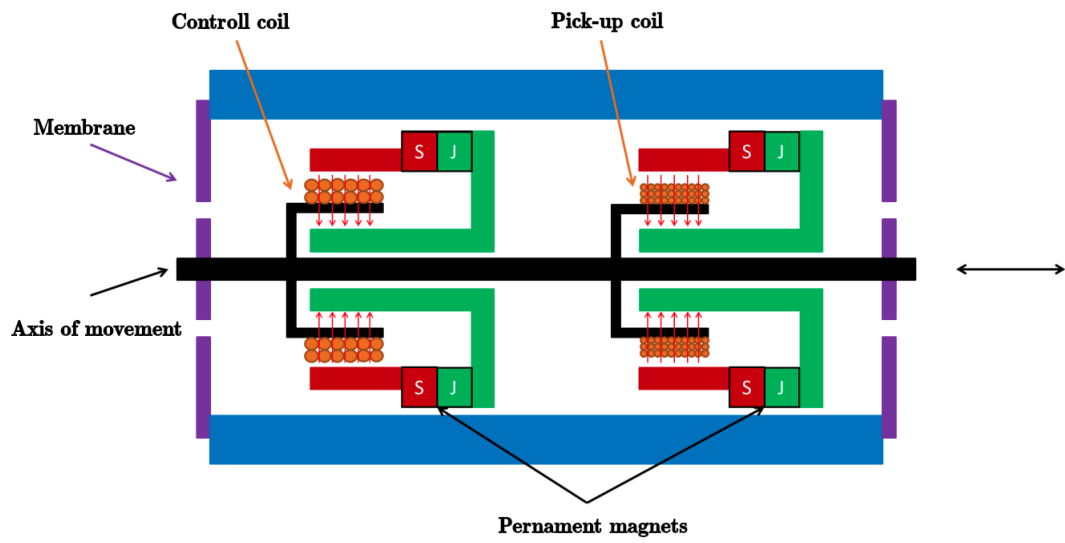


Figure 4.2: Transducer, taken from [2].

The diagram of the MS setup can be seen in the Figure 4.3.



Figure 4.3: Diagram of the MS setup.

## 4.4 MS spectra quality parameters

The MS spectra shape can be modelled by Lorentzian curves. The singlet spectra in transmission geometry can be modelled by a single Lorentzian curve in the following form:

$$L(v) = -I \frac{\left(\frac{\Gamma}{2}\right)^2}{(v - v_0)^2 + \left(\frac{\Gamma}{2}\right)^2} + B \quad (4.1)$$

Where  $I$  is the amplitude, the  $\Gamma$  is the FWHM, and the  $B$  is a background level. The Lorentzian in this form has the associated area  $A$  equal to:

$$A = \pi I \Gamma \quad (4.2)$$

There are two properties of MS spectra which characterize its quality: SNR and the Effect  $E_{\text{MS}}$ . They can be calculated from spectra parameters by following equations:

$$\text{SNR}_{\text{MS}} = \frac{I}{\sqrt{B}} \quad (4.3)$$

$$E_{\text{MS}} = \frac{I}{B} \quad (4.4)$$

# Chapter 5

## Electronics for signal readout and analysis

The signals coming out the detector has to be properly preamplified, amplified and shaped. This task requires special analog circuits with properly designed layout. In our case, we use instruments, modules and parts from two companies - ORTEC and CREMAT. When designing the spectrometric measurement chain, we select components in order to achieve sufficient parameters for our application - energy resolution, low dead time to increase maximum possible counting rates e.g.

The task of realizing the spectrometric chain can be fulfilled in two ways. The first and more straightforward way is to build it from stand-alone robust instruments and modules. This can be more practical approach for testing of the detectors themselves since we are not forced to solve problems arising from badly designed electronic circuits. However, these modules are usually very expensive, measurement setups build this way are unnecessarily large and have worse noise parameters than electronic circuits specially tailored for the given application.

The second possibility is to design printed circuit board (PCB) with required functionalities from electronic parts, However it requires many electronic engineering skills and additional time for development. The analog PCBs are very hard to design. The pros are that the final product can be very compact, and the electronic parts and PCB manufacturing is much cheaper. In this thesis, we apply both methods for the development.

### 5.1 PIN detector connection and support electronics

#### 5.1.1 Voltage source

The PN and PIN detectors require voltage bias to reduce the capacitance. These voltage sources don't have to be stiff since the detector's current consumption is very low.

Gas and scintillation detectors usually require high voltage source (hundreds or thousands of volts). These high voltages are usually supplied by switching power supplies. However, these supplies are usually very noisy and since the semiconductors can be operated at much lower voltages, there is no need for them. The better alternative is charge pump build of capacitors and diodes, which requires lower frequencies to operate.

### 5.1.2 Shielding and grounding

In case of sensitive analog signal circuits, the electromagnetic shielding is a very important part. Sensitive circuits have to be surrounded by a metallic material from all sides, which is also correctly connected to GND (principle of the Faraday cage), otherwise the proper functionality can not be guaranteed. The electromagnetic field from an outside source usually induces currents in the shielding material, and thus the special care has to be taken to prevent these induced currents from flowing through the signal routes. The figure 5.1 shows the difference between correct and wrong connection of shielding.

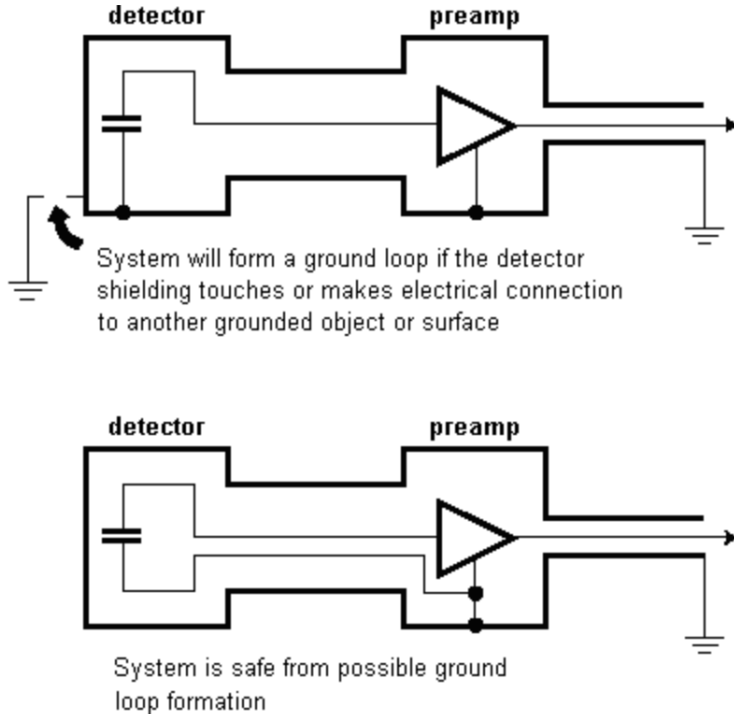


Figure 5.1: Schematic of wrong and correct connection of shielding [22].

### 5.1.3 Cooling

To reduce thermal noise and achieve better SNR it is necessary to cool the detector. The cooling can be achieved by various ways. In most setups, the appropriate solution can be provided by a peltier cooler. These setups with peltier are the easy to implement, however, their cooling efficiency is highly dependent on the ability to sink the heat from the hot side.

## 5.2 Spectrometric chain

The measurement chain for gamma spectroscopy is usually realized in following order - gamma detector, preamplifier, amplifier, multichannel analyser (MCA), microprocessor/computer.

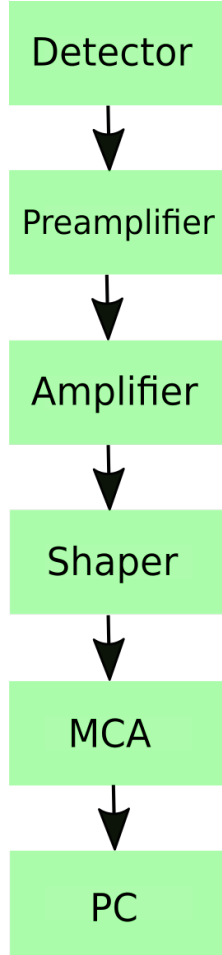


Figure 5.2: Spectrometric chain.

### 5.2.1 Pre-amplification

The signal coming out of the PIN detector is weak, and it is also in form of charge (current pulse), so it is necessary to convert it into voltage pulse. For performing the charge-voltage conversion, one and the best solution is circuit called charge amplifier (also referred as a preamplifier). The principal functional scheme can be described by one opamp with a capacitor in feedback. The functionality is similar to  $I/U$  transimpedance amplifier, but the charge amplifier works mainly as an integrator. In ideal case (opamp amplification  $A \gg 0$ ), the measured voltage per unit charge is approximately equal to:

$$\frac{dU}{dQ} = \frac{1}{C_f}. \quad (5.1)$$

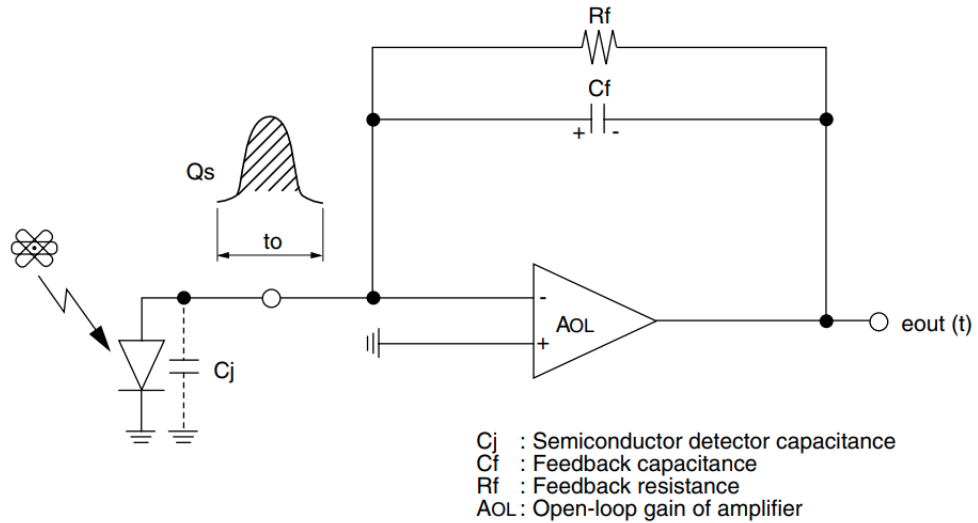


Figure 5.3: Charge amplifier.  $Q_s$  is total charge of pulse and  $t_o$  is the interval of charge generation inside the detector. Taken from [19].

In real circuit there is also a resistor parallel to the feedback capacitor. The feedback resistor slowly discharges the capacitor after a accumulation of charge, restoring the transimpedance amplifier to be ready to capture another pulse.

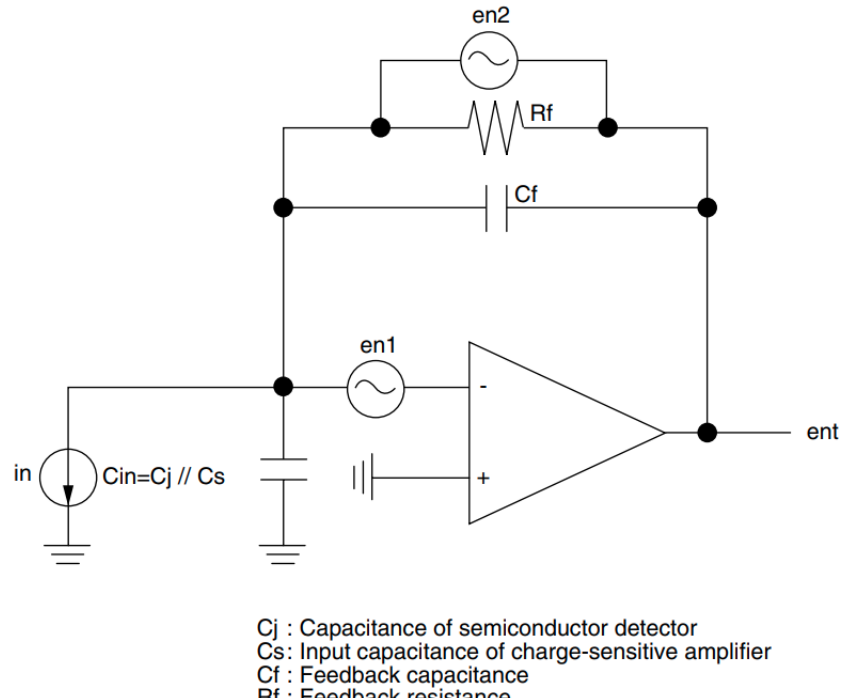


Figure 5.4: Noise equivalent circuit for charge amplifier. Taken from [19].

However, the functionality of charge amplifier is also negatively affected by an electronic noise, which depends on the values of the feedback resistance and capacitance and also on the internal parameters of the connected semiconductor detector and FET (field-effect transistor) inside the amplifier.

This electronic noise can be divided into three contributions, each described by equations for noise voltages and currents [19]:

- Thermal noise of first-stage FET:

$$en_1 = \sqrt{\frac{8}{3} \frac{kT}{gm}}, \quad (5.2)$$

where  $k$  - Boltzmann constant,  $T$  - absolute temperature and  $gm$  - transconductance of FET.

- Shot noise caused by FET's gate current and detector's dark current:

$$in = \sqrt{2e(I_G + I_D)}, \quad (5.3)$$

where  $e$  - elementary charge,  $I_G$  - gate leakage current of first-stage FET and  $I_D$  - dark current of detector.

- Thermal noise caused by feedback resistance:

$$en_2 = \sqrt{4KTR_f}, \quad (5.4)$$

where  $R_f$  - the feedback resistance.

The square of total noise  $ent^2(j\omega)$  is given by equation:

$$ent^2(j\omega) = en_1^2 \cdot (1 + \frac{C_{in}}{C_f})^2 + \{in^2 + (\frac{en_2}{R_f})^2\} \frac{1}{(j\omega C_f)^2}, \quad (5.5)$$

where the  $C_f$  - the feedback capacitance and  $C_{in}$  - the total input capacitance, resulting capacitance on the input of amplifier (there - parallel combination of detector's capacitance  $C_d$  and amplifier's input capacitance  $C_s$ ).

The first term in equation 5.5 depends on the ratio between the input capacitance  $C_{in}$  and the feedback capacitance  $C_f$  and thus the preamplifier's feedback capacitance has to be optimized in order to reduce the electronic noise.

The charge sensitive preamplifiers modules usually also contain the second stage - common voltage amplifier. The internal scheme of CR-110-R2 charge amplifier made by Cremat Inc., which we use in the case of PCB design can be seen In the Fig. 5.5.

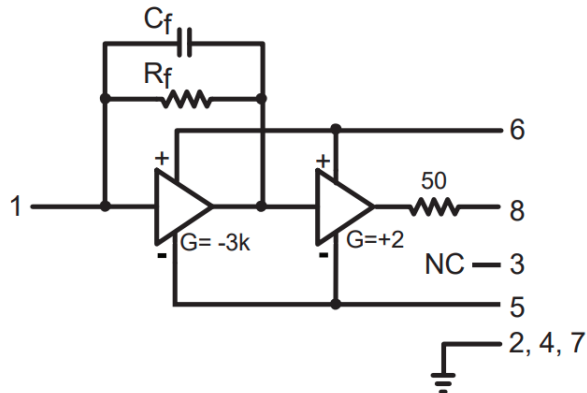


Figure 5.5: Internal scheme of CR-110-R2 charge sensitive preamplifier [23].

The output voltage has the shape of exponential decay with amplitude defined by energy deposited into detector, short rise time (in orders of nanoseconds) and a longer decay constant (microseconds).

CR-110-R2 offers the conversion gain  $G = 1.4 \text{ V/pC}$ , decay constant  $\tau = 140 \mu\text{s}$  CR-110-R2) and noise (FWHM) in silicon equal to 1.7 keV [23]. It can be easily calculated, that for 14.4 keV photon, the output pulse has amplitude equal to  $U_A = 0.8928 \text{ mV}$ . Note that the noise caused by the preamplifier is much larger than the intrinsic fano noise (FWHM = 185.4 eV).

The modular version suitable for our application is ORTEC 142A charge preamplifier with  $G = 1.016 \text{ V/pC}$ ,  $\tau = 500 \mu\text{s}$  and noise in silicon equal to 1.6 keV [32]. Charge preamplifiers are usually very sensitive devices and can be very easily damaged by electrostatics.

Since the output of preamplifier is in order of millivolts, it has to be strongly amplified. Very fast and low noise amplifier consisting of multiple opamps is an appropriate solution of this problem.

### 5.2.2 Shaping

To perform the accurate energy discrimination, the pulse shape has to be altered from exponential decay shape by a shaping circuit. The shaping results into filtering the frequency band (reducing the noise) and also into shortening the long decay times of original exponential shapes. The shorter duration of pulses prevents the negative effect in which one pulse superimposed onto another (pile-up effect).

The Gaussian shape meets the sufficient parameters of SNR and duration [30]. This type of shaping is usually achieved by several integration stages. The Cremat module CR-200-1us-R2.1 offers gaussian shaping with shaping time 1  $\mu\text{s}$  [24]. Its simplified internal schematic can be seen on fig.5.6.

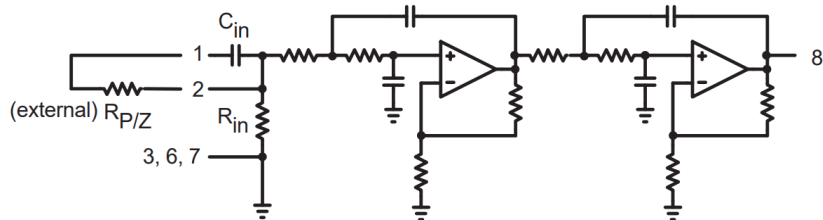


Figure 5.6: Internal scheme of CR-200 Gaussian shaping amplifier [24].

However, shapers are usually very sensitive on the shape of the input pulse. They expect step-like input pulse. The deviation from the expected shapes may result into undefined shapes on output of the shaper. In modules the shapers are usually integrated along with amplifiers.

### 5.2.3 Multichannel analysis (MCA)

To obtain the full energy spectra information, it is necessary to measure and digitize pulse height of incoming pulses to perform energy discrimination and increment the corresponding channels. The multichannel analyser (MCA) can be employed for these purposes. The EASY-MCA-2K from ORTEC [29], which we use in experiments, is

capable of processing Gaussian shaped pulses with shaping times from  $0.25 \mu\text{s}$  to  $30 \mu\text{s}$  and amplitudes ranging from 0 to +10 V.

# Chapter 6

## Gamma spectrum software analysis

As was mentioned before in section 1.2.2, the measured gamma spectrum contains many unwanted artifacts like noise, Compton continuum and edges and additional peaks created by various interactions. To properly obtain the count rates on defined energies, the only way is to perform a numerical analysis of measured data. Locations of energy peaks are to be found for example by their characteristic second derivatives. Absolute count rates are then obtained by Gaussian fitting.

### 6.1 Peak searching procedure

Many commercial programs use peak searching procedures based on algorithm originally developed by M.A. Mariscotti [3]. This method is based on the numerical second difference assuming that the background can be approximated only by linear functions and thus it vanishes in case of the second derivative. The second fact is that the searched peaks are Gaussians with their specific second derivatives and thus their positions can be found in local minimums (Gaussians have negative second derivatives since they are concave functions). To reduce noise, the second difference is averaged by defined number of steps.

To determine if the found minimum should be considered as peak position (not as a Compton edge etc.), standard deviation and other additional rules based on number of points in specified intervals can be employed. However, algorithm needs input parameters, which are based on raw estimation of FWHM of searched peaks.

For the analysis of measured gamma spectra, this algorithm was implemented in C++ and used to find full energy peaks and other additional peaks as well. The following figures show the example of measured spectra and its second difference plotted along with its standard deviation. The possible candidates onto peak positions can be observed.

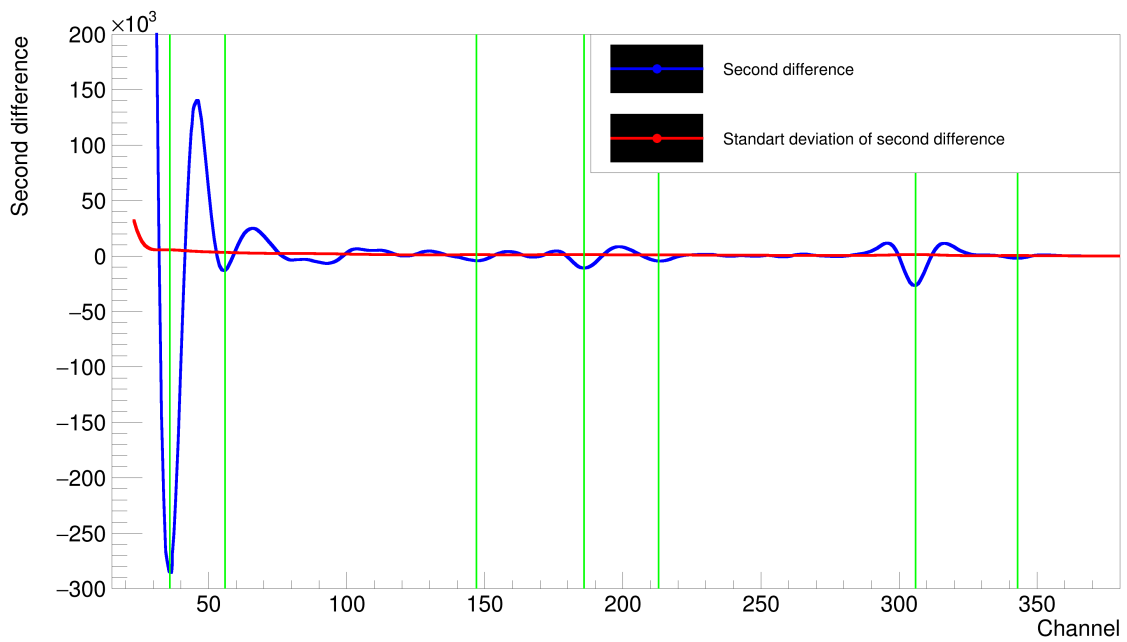


Figure 6.1: Second difference of example spectra along with its standard deviation showing possible candidates (green lines).

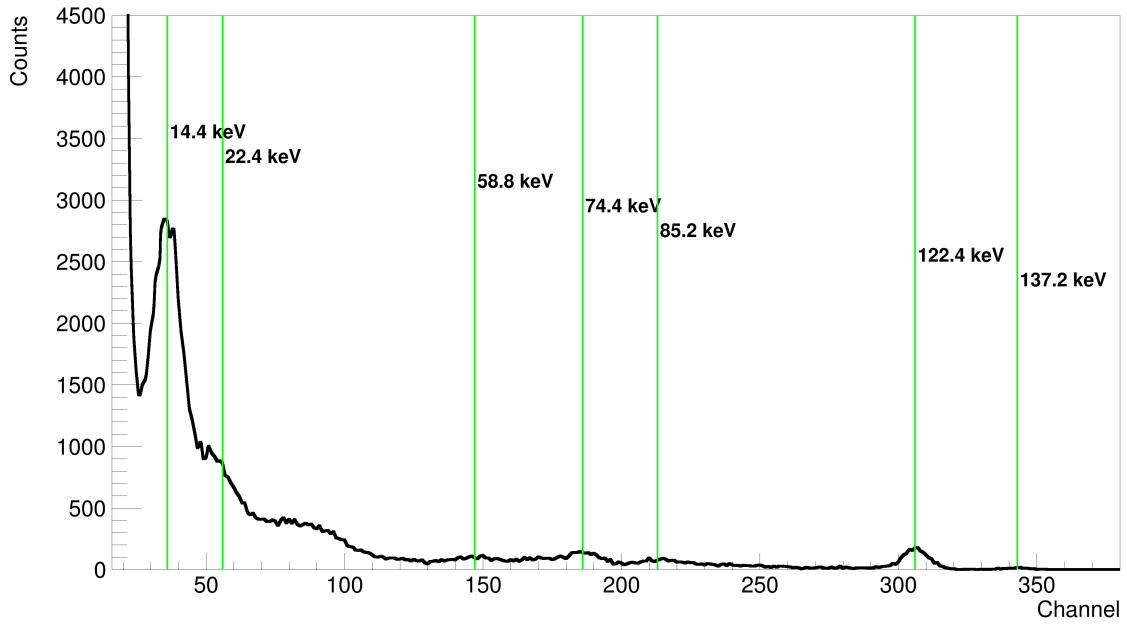


Figure 6.2: Example of measured gamma spectra. Green lines mark the energy peaks found by algorithm.

# Chapter 7

## Gamma detection testing

The purpose of this experiment is to determine the necessary conditions under which the gamma spectroscopy with selected photodiodes can be performed and find out whether the photodiodes are even capable of detecting gamma rays since some of them are not determined for detection of gamma rays. The determination of detection efficiency is precisely done in following chapters for selected photodiodes.

For the very first test of photodiodes we assembled a spectrometric setup from ORTEC modules including preamplifier ORTEC142A, shaping amplifier 575A and high voltage power supply 556 inside the ORTEC minibin. The pulses were captured by EASY-MCA-2K from ORTEC connected to PC running the MAESTRO Multichannel Analyzer Emulation Software [31]. As radiation source we used  $^{57}\text{Co}$  50 mCi Mössbauer source from 2016. It was also necessary to cover the part with radiation source with lead shielding blocks.



Figure 7.1: ORTEC minibin with MCA connected to PC.



Figure 7.2: PIN diode inside the shielding crate connected to the preamplifier to measure the spectrum of  $^{57}\text{Co}$  source with filter.

## 7.1 Noise and its reduction

When performing gamma spectroscopy measurements, the energy spectra are affected by noise. In order to reduce noise as much as possible, two approaches were tested - shielding the detector by various ways and cooling to temperatures near 0 °C.

### 7.1.1 Electromagnetic noise reduction

Photodiodes have to be sufficiently electromagnetically shielded and their distance to the preamplifier input should be as short as possible. Using the diodes with poor shielding leads into high levels of electromagnetic noise, which make mayor part of energetic spectra unobservable.

Based on many test it was proven that the optimal way to shield the photodiode is to put it into the aluminium crate (see Figure 7.3). This crate has to be as small as possible and has to be connected to the grounding potential. However, the front side of the crate has to be open to allow the sufficient transmission of gamma photons to the detector. To preserve the shielding properties, this drilled hole has to be still covered by a conductive material. Our choice was a thin aluminium foil, which has sufficient gamma transmission parameters as well as electromagnetic shielding parameters.



Figure 7.3: Photodiodes inside aluminium shielding crates.

### 7.1.2 Thermal noise reduction

To reduce the thermal noise, the S14605 photodiode was cooled by ice. It was placed in shielding box, which had attached heat sink to the bottom. This heat sink was submerged into the small tub filled with an ice (see Figure 7.4). The thermal conduction was improved by sticking the photodiode to the floor of the shielding box by a conduction paste. The photodiode was cooled this way to temperatures around 7-8 °C.

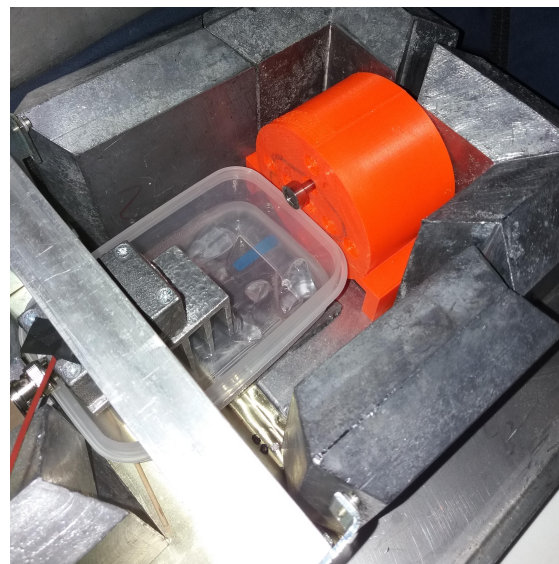


Figure 7.4: Detector cooled by ice.

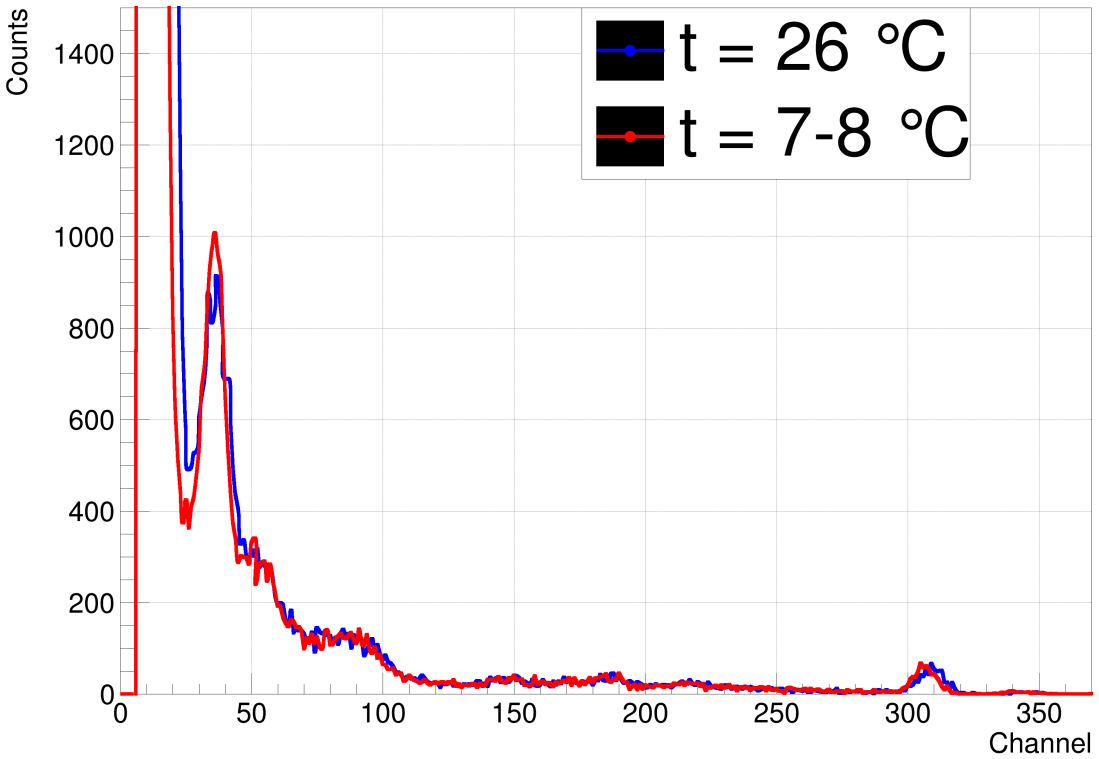


Figure 7.5: Measured  $^{57}\text{Co}$  spectra at two different temperatures.

The results show that the cooling improves SNR, but its effect is small when compared to the effect of proper shielding. The cooling is not used in following tests on ORTEC setup.

## 7.2 Detection test of the $^{57}\text{Co}$ spectra

The spectra for every photodiode were taken for 30 min of real time (MCA allows dead time compensation) with the source's distance 1 cm from the front shielding crate. There is a simple test with a set of filters, which can help us to find out the corresponding energies to the measured peaks:

- Pb filter: everything should be attenuated.
- Cu filter: transmitted - 122.1 keV, 136.5 keV not transmitted - 14.4 keV, 6.4 keV.
- Al filter: transmitted - 122.1 keV, 136.5 keV, 14.4 keV not transmitted - 6.4 keV.

The analysed spectrum is analysed by our peak finder program (described in section 6.1) to find the characteristic energy components. By filter test it can be determined which peak corresponds to 14.4 keV (Cu - attenuated, Al - not attenuated). The channel position of 14.4 keV is then used to calibrate the energy axis of the MCA spectrum.

The Compton edge caused by interaction of 122.1 keV photons inside the detector can be expected. The equation 1.8 estimates the position to be around 39.5 keV.

### 7.2.1 S14605 test

From the S14605 capacity and dark current graphs (data-sheet ??) can be deduced optimal voltage. We decided to set it to 50 V, because any further increase of voltage does not improve the SNR. The measured spectra with no filter, with particular filters and only background (fully shielded) are in the Fig. 7.6.

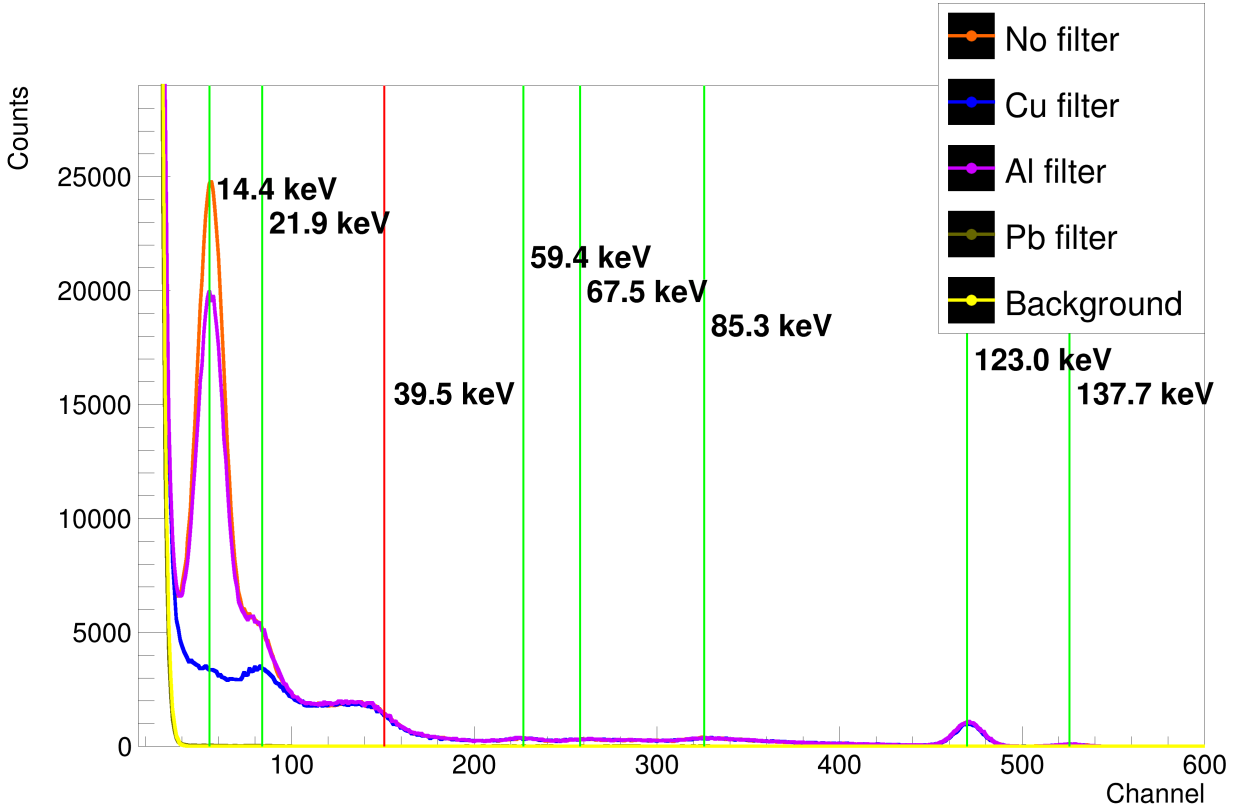


Figure 7.6: S14605 spectra with founded energy peaks (green lines) and estimated Compton edge (red line).

Due to the first peak's attenuation by mentioned filters, this peak is determined as 14.4 keV full energy peak. The 21.9 keV peak originates from characteristic x-rays of rhodium matrix. 59.4 and 67.5 keV 85.3 keV is characteristic x-rays of lead shielding. The last two peaks (123.0 keV, 137.7 keV) are from  $^{57}\text{Co}$ . It can be seen that the full energy detection efficiency of higher energies (122.1 keV) is very small and that the Compton scattering is preferred interaction effect inside detector at these energies, which results into expected Compton edge. The expected peak of 6.4 keV hidden in the electronic noise. The modular ORTEC setup do not allows any further upgrades, so the only way to improve SNR is to integrate the spectrometric chain into PCB.

### 7.2.2 BPW34 test

The instrumentation was similar as before, but BPW34 had to be operated at lower bias voltage and thus 20 V was chosen as an optimum.

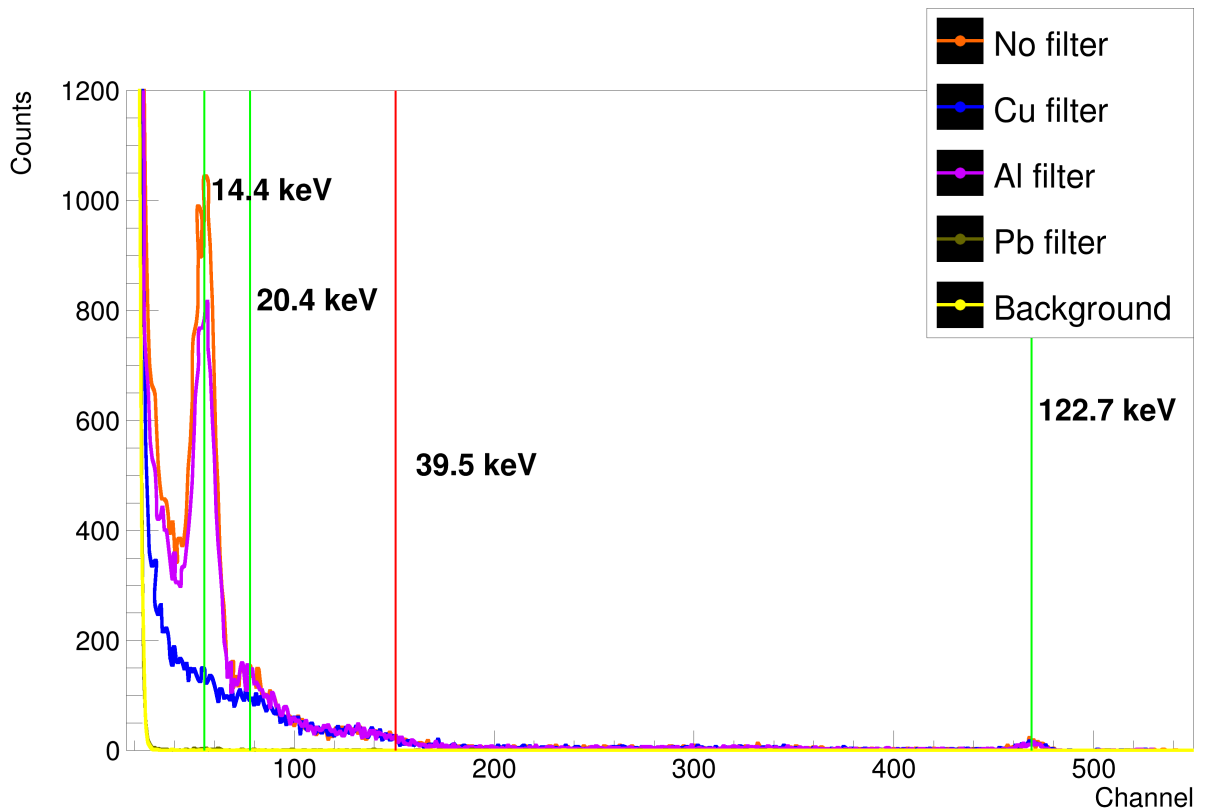


Figure 7.7: BPW34 spectra with founded energy peaks (green lines) and estimated Compton edge (red line).

The measured spectra of BPW34 is very similar to the previous one, however the peak's heights are approximately 25 times lower.

It is surprising that this cheap photodiode is capable of capturing gamma rays with sufficient energy resolution.

### 7.2.3 OPF430 test

OPF430 was operated at 20 V. There was a problem with the very low detection efficiency, so the source had to be put into the shielding box right before the photodiode.

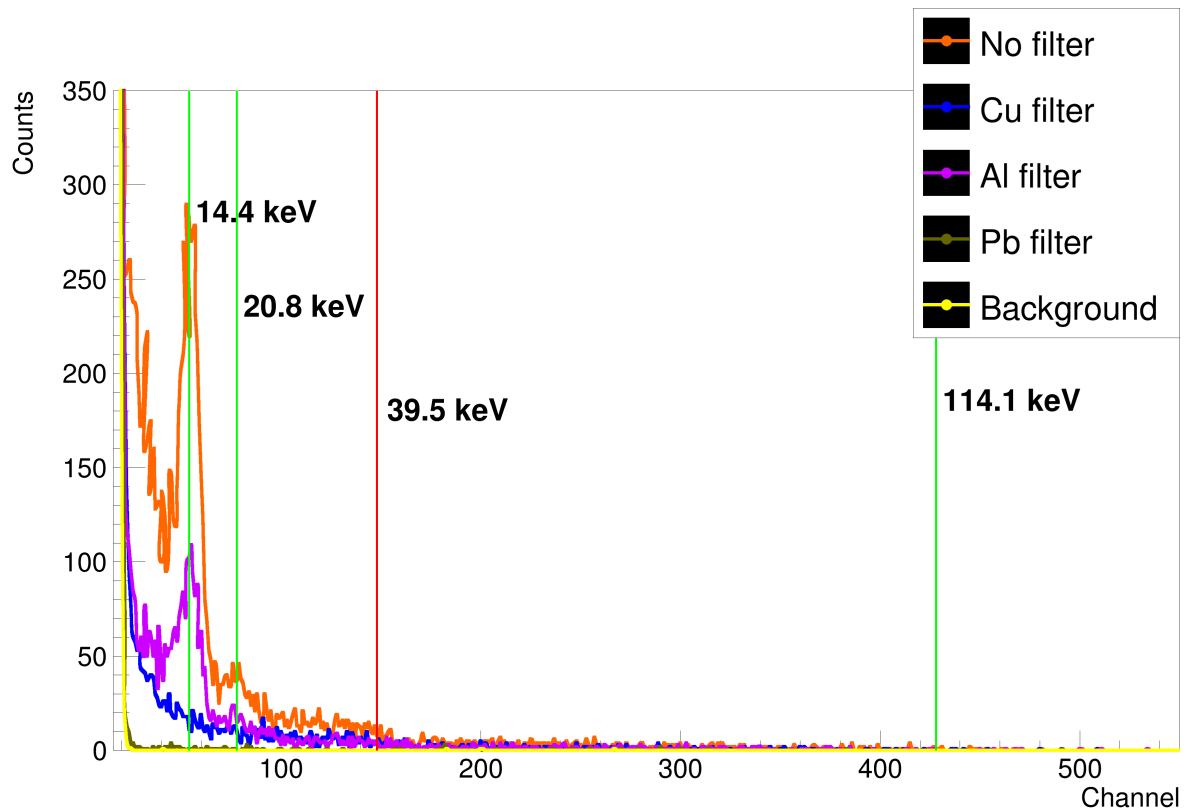


Figure 7.8: OPF430 spectra with founded energy peaks (green lines) and estimated Compton edge (red line).

It can be seen that the count rates are still much lower than they were measured at previous photodiodes. This is probably due to the fact, that the surface of detector is very small. The conclusion is that OPF430 is capable of capturing the low-energy gamma rays, however, the efficiency is so bad that it makes it unusable for any real gamma spectroscopy application.

# Chapter 8

## Design of integrated amplifier

The only way to improve the performance of the spectrometric chain is to integrate the amplification part and a shaper into a small PCB - short the signal routes, reduce parasitic capacitances at preamplifier input and improve the shielding. The various prototypes were designed as double-sided PCBs and manufactured by using the milling machine for PCB to remove cooper from cuprexit plates. The PCB consisting mainly of surface mount deposition (SMD) parts was then assembled by manual soldering.

### 8.1 Scheme and layout

The main parts of spectrometric chain integrated PCB are: photodiode input connector, preamplifier, second stage amplifier, shaper module, output buffer optimized for  $50\ \Omega$  transmission line, bipolar voltage supply for modules and bias voltage supply for photodiode. To surround the sensitive parts with sufficient shielding, the PCB is placed into aluminium box with drilled photodiode window. The full schematic of the integrated amplifier can be seen in the Fig. 8.3 and the real layout for PCB can be seen in the Figures 8.4 and 8.5.

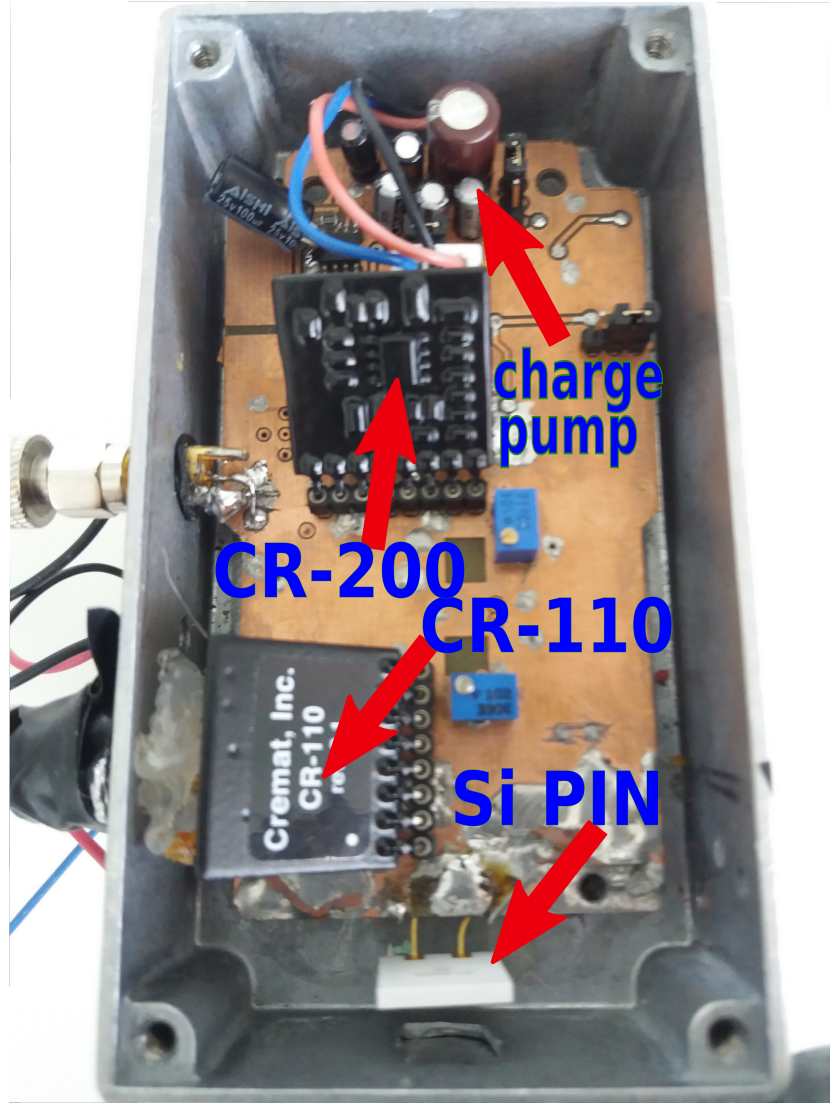


Figure 8.1: Fully assembled PCB with attached cremat modules inside the shielding box.

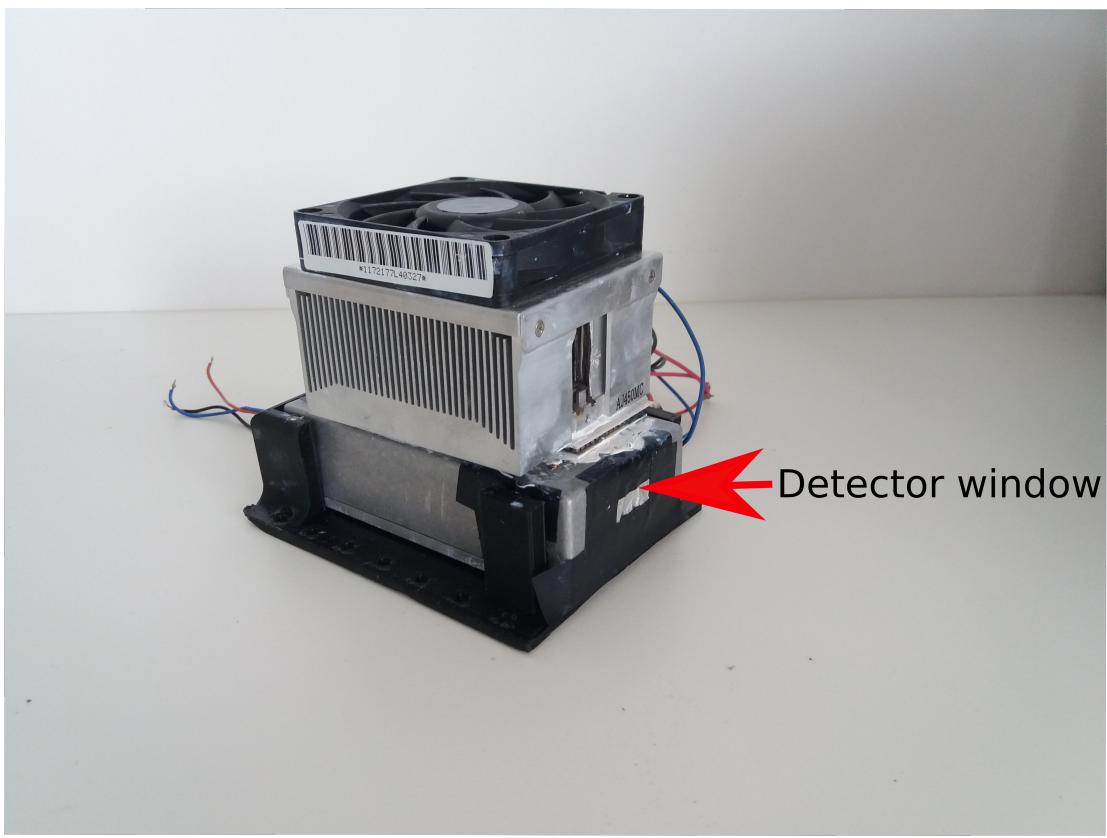


Figure 8.2: PCB in aluminium box with attached peltier coolers.

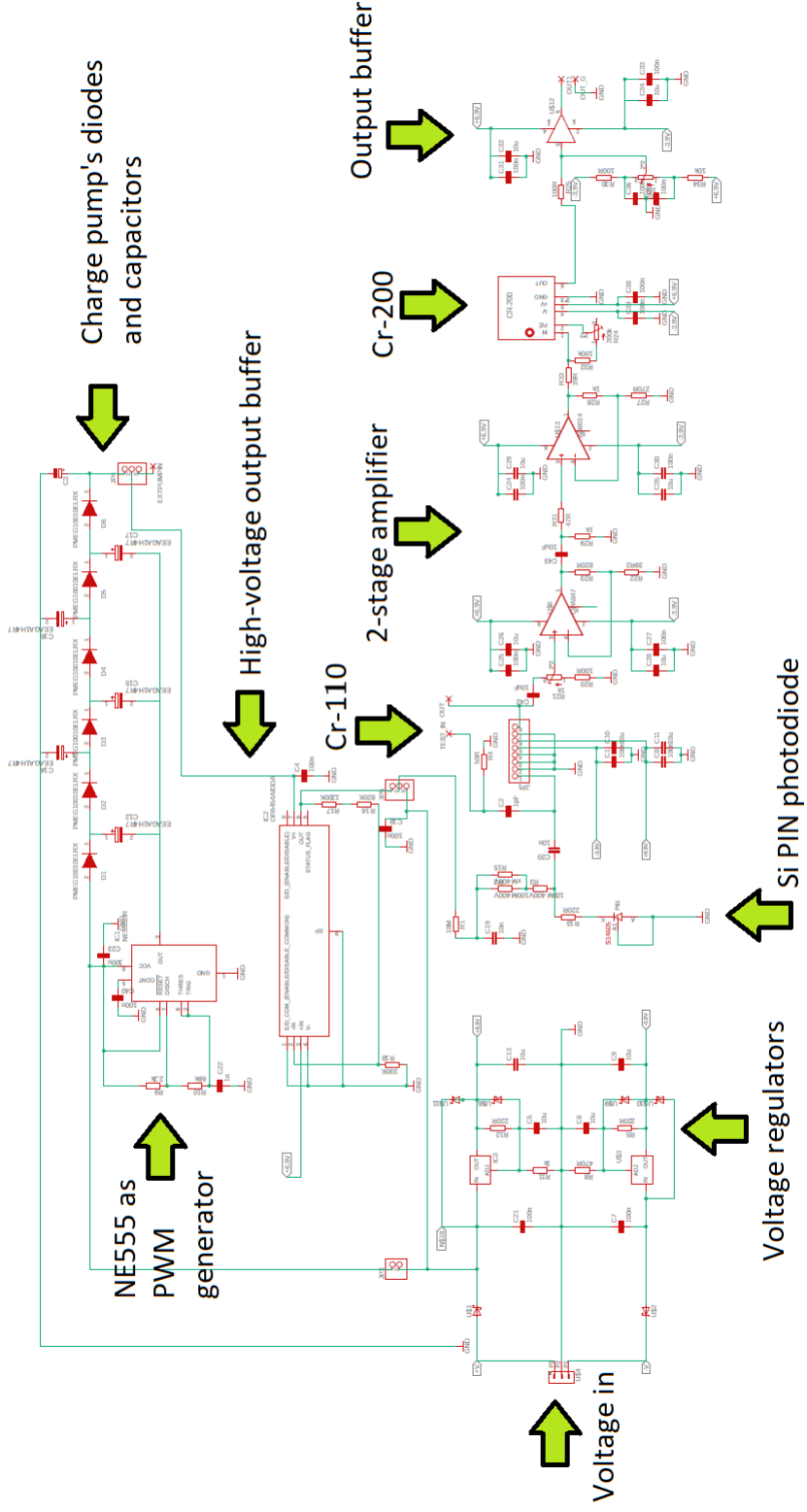


Figure 8.3: Schematic of spectrometric chain PCB designed in EAGLE [12]. Full schematic can be found in attachments.

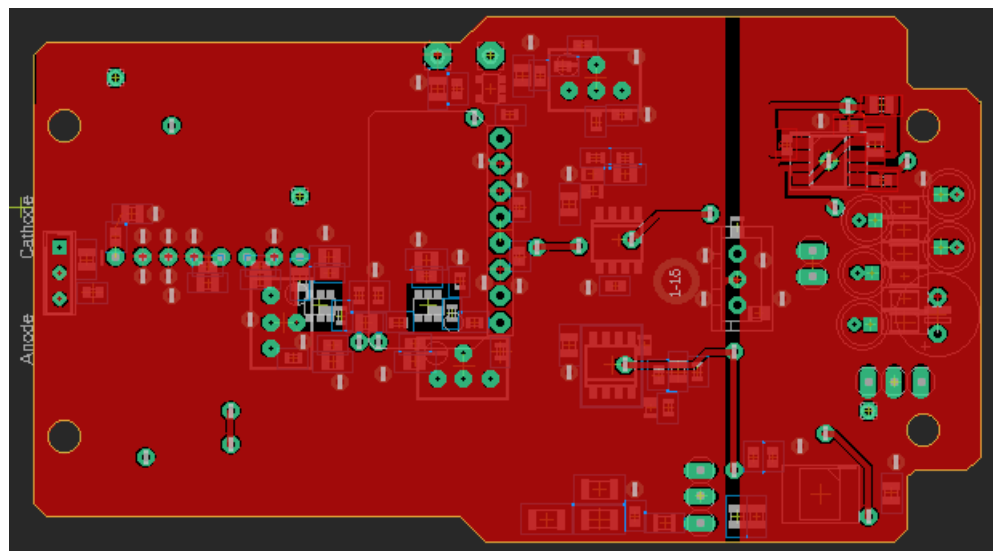


Figure 8.4: Layout of spectrometric chain PCB designed in EAGLE [12], top side layer.

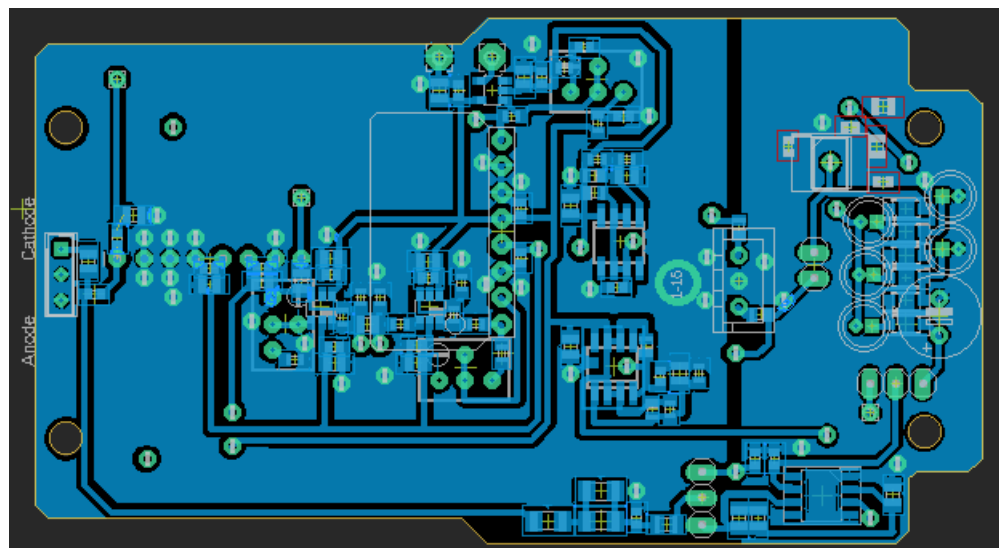


Figure 8.5: Layout of spectrometric chain PCB designed in EAGLE [12], bottom side layer.

## 8.2 Grounding and Shielding

To allow all the currents to have their return path with a sufficient conductivity, the main GND signal has to be spilled all around the circuit board. Even a small resistances in these paths may cause additional noise in signals. Currents from non-signal parts such as charge pump should have their return path different from the path of signal parts, and thus the spilled GND has to be cut to several separate parts connected together only at input voltage connector. This kind of layout is referred as a star ground structure [25].

The shielding box has to be connected to GND in carefully selected place to prevent the induced currents from shielding to flow over the signal ground of the detector. The best place to connect the shielding box with GND is near the input voltage connector.

## 8.3 Photodiode input and preamplifier

The photodiode is situated inside the box, and the cathode is connected to bias voltage and to preamplifier (CR-110) by capacitive coupling (10 nF capacitor). CR-110 application note also mentions an optional  $220\ \Omega$  resistor connected before coupling capacitor to prevent CR-110 breakdown by large current spikes. Our experiences show that this resistor should not be omitted.

The signal route has to be as short as possible. The layout should also be designed in ways to reduce the parasitic capacitances at the preamplifier input - the copper connected to ground (GND) should be removed from areas around the signal input route and around input bias voltage route.

## 8.4 Amplification

The preamplifier output is routed over capacitive coupling (to eliminate unwanted offset) and over potentiometer divider (to adjust signal amplitude) to the amplification stages.

First amplification is achieved by two non-inverting amplifiers with OPA847 opamps. Each stage has the amplification of  $32\times$  (or less, this is different for every of our prototypes). Additional amplification  $10\times$  is done by shaper module CR-220. The OPA847 opamp datasheet [26] describes that these fast opamps are prone to unwanted oscillations, and therefore the GND around the opamp must be removed from both sides of the PCB. The output of shaper module is routed directly to output buffer opamp Max4201. The end of chain is buffered and connected to the output SMA connector mounted onto the aluminium box.

## 8.5 Voltage supply

The regulation of power supply (usually +15 V and -15 V) is done by LM317 and LM337 regulators, which convert input supply voltages into +7 V and -4 V. The output voltage of regulators is set by two resistors. However, these regulators produce heat, which negatively affects the SNR, so this heat has to be taken out of the circuit board by the thermal bridge connection to the aluminium box. To stabilize the temperature during the long runs, the shielding case has two additional peltier couples with fan attached onto it.

S14605 requires bias voltage around +50 V, which can be supplied by 3-stage charge pump, assembled simply from capacitors, diodes and PWM generator - for example NE555. The charge pump is theoretically designed to multiply the input voltage +15 V to +60 V. However, due to the fact that the rectifying diodes have some dropout and also because the charge pump is not a stiff voltage source (even a small currents cause large dropout), the real bias voltage is around +50 V. The pump's output has to be filtered, because it can contain voltage spikes from switching frequency (NE555's frequency is set to 10 kHz). To filter this high voltage output the high-voltage opamp OPA454 is connected as buffer - the pump's voltage is connected as opamp supply, and the voltage from regulator (+7 V) is connected into opamp negative input pin. There is also a jumper which allows to switch between +15 V (for BPW34 photodiode) and +50 V.

# Chapter 9

## **$^{57}\text{Co}$ spectra measurement with integrated amplifier**

To properly test the assembled PCB with attached S14605 photodiode (further referred as Si PIN detector) and to compare its detection efficiency for 14.4 keV photons with the detection efficiency of the other types of detectors - scintillator and gaseous detectors, the measurement setup with carefully designed geometry was constructed.

The onboard amplification is set in a way to have 14.4 keV energy peak in the second half of the channel range, which on the other hand result into the saturation of the higher energies, but the detection of these energies is not our focus.

### **9.1 Measurement setup**

The measurement setup mainly consist of 3D printed parts - plastic holders for every detector and holders for radiation filters. All the holders have to be modular and easily interchangeable to allow the geometry to be kept same for every detector.  $^{57}\text{Co}$  2020 source is mounted onto the transducer (switched off in this measurement). Due to the fact, that the detectors have a different size of detection area, the irradiation has to be done through a collimator. To compare detection efficiency of the defined detection surface, the detector is irradiated through a hole ( $d = 4$  mm) in a lead shielding, which works as collimator for  $^{57}\text{Co}$  source.

For every detector, the sequence of five measurement was performed - without filter, with three filters and without a source. The relative detection efficiency for 14.4 keV is determined by Gaussian fit of the 14.4 keV peak in spectra with subtracted background. Every measurement of spectra ran 1200 s of live time.



## 9.2 Si PIN detector measurement

The output SMA connector is connected directly to the ORTEC MCA. Three filters were placed before lead collimator - Cu (255  $\mu\text{m}$ ), Al (780  $\mu\text{m}$ ), Pb (5 mm).

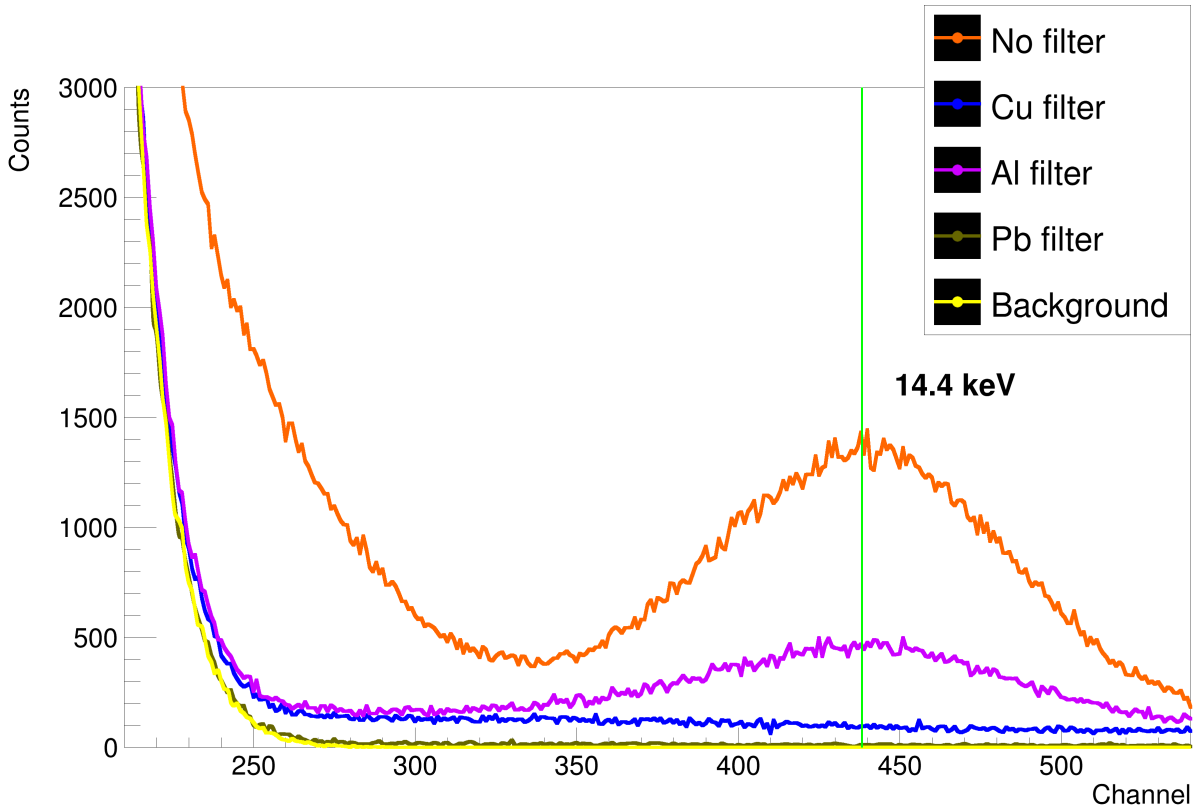


Figure 9.2: Si PIN detector  $^{57}\text{Co}$  spectra.

It can be seen, that the noise in spectrum is much lesser than in case of ORTEC setups. The part of 6.4 keV peak can be also seen. Various ways were performed in order to reduce noise - cooling by ice, improving the shielding etc. However, none of them resulted into 6.4 keV energy peak without noise. Main part of remaining noise probably arises from Si PIN diode capacity ( $C_{\text{Si4605}} \approx 25 \text{ pF}$ ). This fact can be confirmed by using the same PCB with photodiode with smaller capacity (for example BPW34,  $C_{\text{BPW34}} \approx 10 \text{ pF}$ ). Spectra of BPW34 attached to the integrated amplifier can be seen in the Figure 9.3.



Figure 9.3: Spectra of BPW34 attached to the integrated amplifier.

### 9.3 Scintillator and gas detector measurement

To measure the scintillator and the gas detector relative efficiency the same setup was used. As a gas detector was used tube LND45479, optimized for the 14.4 keV detection with amplification electronics based also on Cremat modules. In case of scintillator detector, our choice was photomultiplier tube R6095 [21] with C9028-01 socket [20]. As a scintillator crystal was used 0.4 mm thick YAP(Ce) and the amplification is done by the custom made amplifier[2].

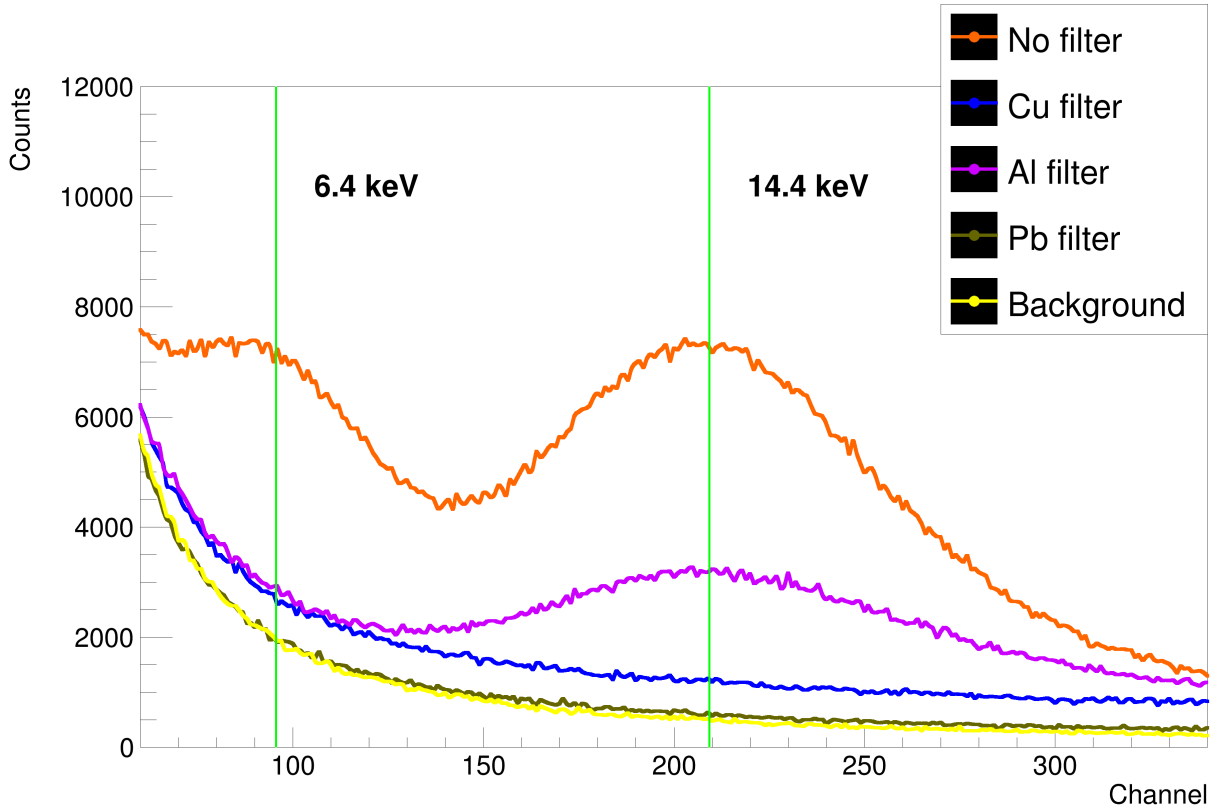


Figure 9.4: Scintillator  $^{57}\text{Co}$  spectra.

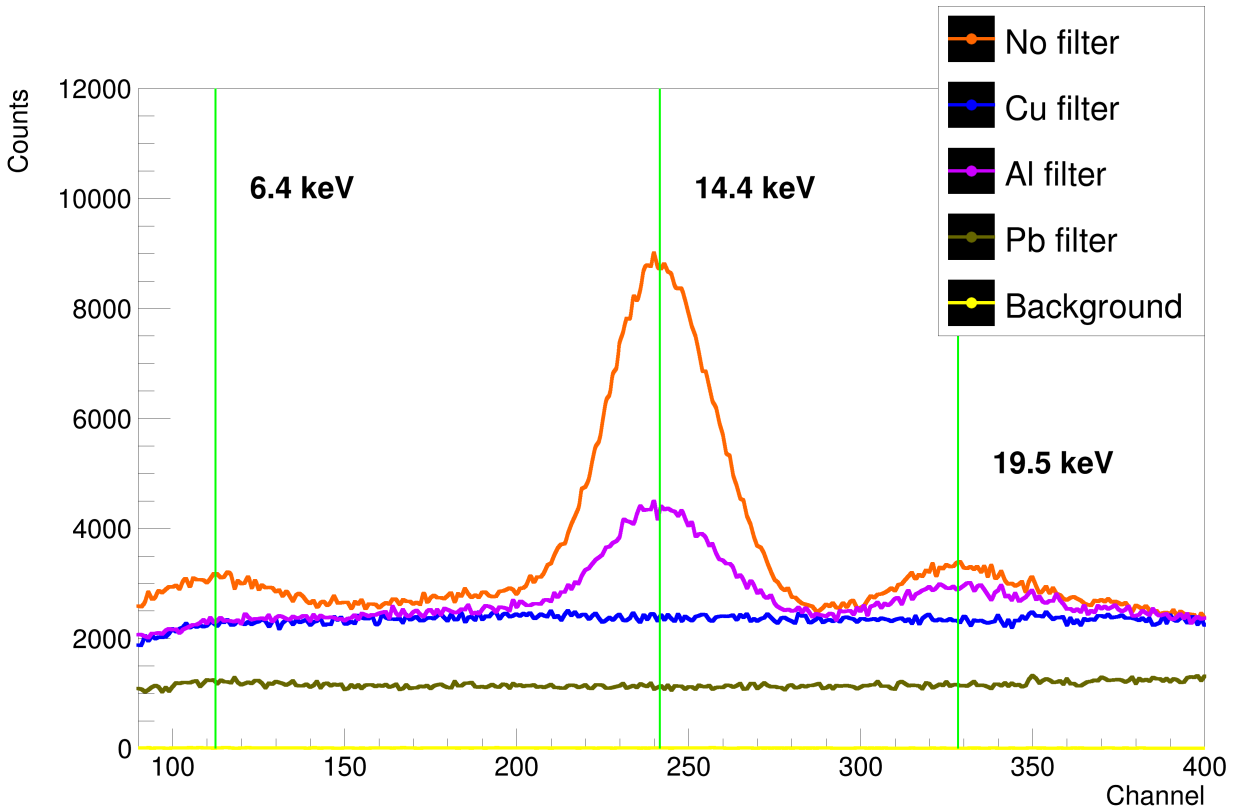


Figure 9.5: Gas  $^{57}\text{Co}$  spectra.

In spectra of gas detector, three narrow peaks can be observed - 14.4 keV peak and two small peaks - 6.4 keV and 19.5 keV. It also has a high level of Compton continuum. The scintillator sees both 6.4 keV and 14.4 keV full energy peaks. However, its energy resolution is much worse - both peaks are noticeably wider and they overlap each other.

## 9.4 Results

The sum of total counts for 14.4 keV and 6.4 keV full energy peaks along with the relative detection efficiency with respect to the most effective detector was calculated in the following way:

1. From the spectra without filter is subtracted the spectra with Cu filter. This provides a sufficient elimination of Compton continuum caused by 122.1 keV photons.
2. The spectra obtained in previous step is fitted by a sum of Gaussians. Spectra of Si PIN and scintillator were fitted by sum of 2 Gaussians and in case of gas, the sum of 3 Gaussians is used.
3. The value of absolute counts (Gaussian's area) for the given energy spectra is calculated from the fit parameters with the uncertainties also taken from the fit.

	absolute	relative
Si PIN	$143000 \pm 3000$	$0.291 \pm 0.008$
gas	$231000 \pm 2000$	$0.48 \pm 0.01$
scintillator	$491000 \pm 9000$	1

Table 9.1: Table of calculated absolute and relative counts of 14.4 keV photons for each detector.

The peak of 6.4 keV photons is not fully observable in the case of Si PIN detector. However, a rough estimation can be calculated using parameters obtained from Gaussian fit of partial 6.4 keV peak. Results in table 9.2 are considered to be only indicative. Note also that the setup wasn't designed to detect 6.4 keV photons - some detectors have slices of Al coating in detector window (Si PIN - ,scintillator - ,gas - window made of unknown metal).

	absolute	relative
Si PIN	$273000 \pm 8000$	1
gas	$20000 \pm 4000$	$0.07 \pm 0.02$
scintillator	$184000 \pm 5000$	$0.68 \pm 0.03$

Table 9.2: Table of calculated absolute and relative counts of 6.4 keV photons for each detector.

The results in table 9.1 show that the scintillator detector is the best detector for 14.4 keV photon among the three detectors that were tested. The Si PIN detector does not excel in detection of these energies and can be classified as the worst of the three. However, by the information provided by S14605 datasheet [17], we come to a conclusion that the efficiency at 6.4 keV energies can be about 51 % better. This can be partially confirmed by rough estimations in table 9.2, which describe the Si PIN as the best detector for 6.4 keV photons. To measure the full peak of 6.4 keV photons with S14605 photodiode, upgrades in electronics have to be made in order to increase the SNR, mainly the preamplifier has to be optimized for S14605's capacitance.

# Chapter 10

## Mössbauer spectra measurement

The previous chapter compared the three detectors in detection efficiency of 14.4 keV photons. This chapter compares them in an efficiency of measuring the MS spectra.

The good detection efficiency of 14.4 keV photons does not necessarily imply the good efficiency of MS spectra measurement and vice versa. Effects, which are not corresponding to the full 14.4 keV photon detection (for example Compton continuum) and generate counts at the channel interval selected for MS measurement, decrease the SNR of MS spectra. To determine this efficiency, setup similar to the one intended for MCA measurement is used again, however, additional parts has to be employed such as a moving transducer and a sample placed into a sample holder. As a sample for this measurement was chosen  $K_3[Fe(CN)_6]$ , which is characterized by a singlet spectrum.

The entire MS setup is controlled by the special control unit controlled by PC software [**MSControl**], both developed on DEP. Control unit drives the transducer, regulates its velocity and also processes the incoming pulses from the detector. The control software also takes care of all the data processing and produces MS spectra data files, which are analysed in this chapter.

The detector's output is routed directly to the MS spectrometer control unit, where the channel interval for MS spectra measurement is selected. However, the previous MCA showed that the interval of 14.4 keV peak is different for every detector, so, to compare the detectors in MS efficiency, the channel interval has to be selected according to the location of 14.4 keV energy peak. We selected this interval as 90% of FWHM of 14.4 keV energy peak with respect to the results of MCA measurement for each detector.

$^{57}\text{Co}$  radiation source is mounted onto the moving part of transducer of the "piglet" type also developed on DEP. The transducer is very sensitive to the vibrations and thus it requires to be placed on the soft mat along with the detector and the sample holder. Before the measurement, the velocity calibration routines provided by control SW have to be performed on the transducer to obtain the scaling coefficient which is then used to recalculate the velocity axis from the arbitrary units into the  $\text{mm}\cdot\text{s}^{-1}$ .

The three measurements (figures 10.1, 10.2 and 10.3) were performed with the calibrated transducer, one for every detector. One MS spectra was measured for 20 hours including only the valid cycles when the velocity error did not exceed the defined limit.

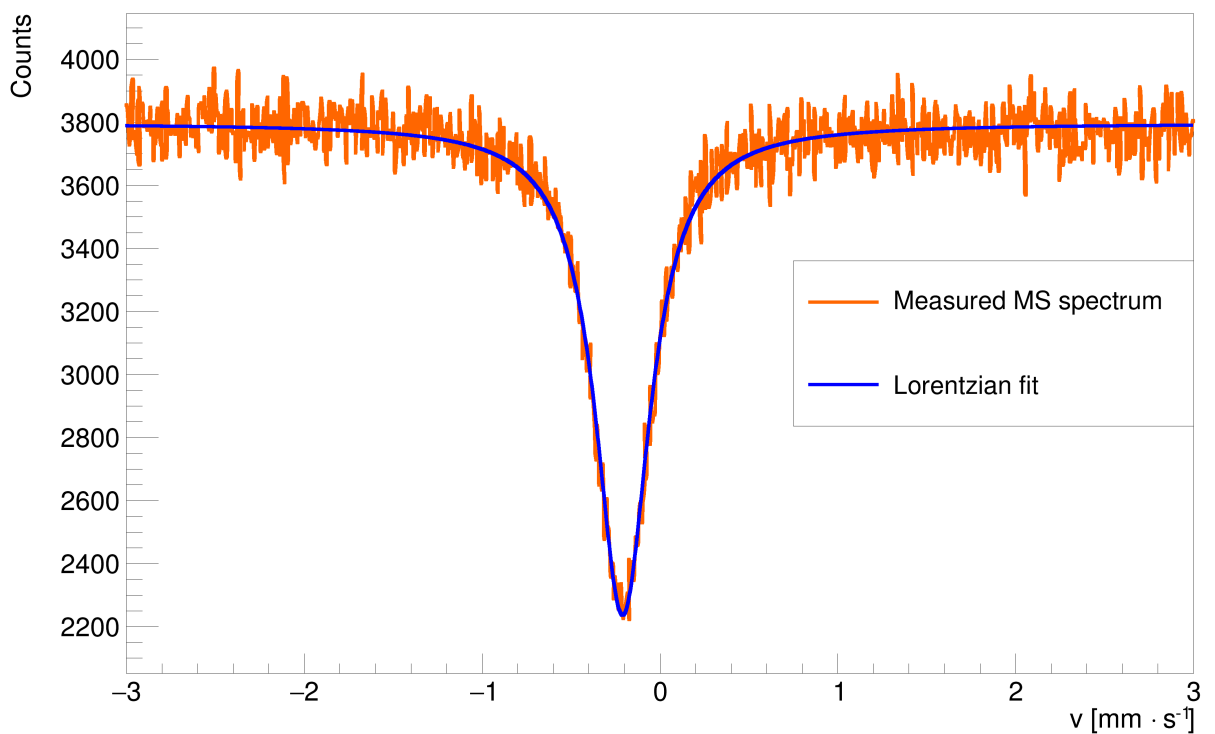


Figure 10.1: Si PIN detector  $\text{K}_3[\text{Fe}(\text{CN})_6]$  MS spectra.

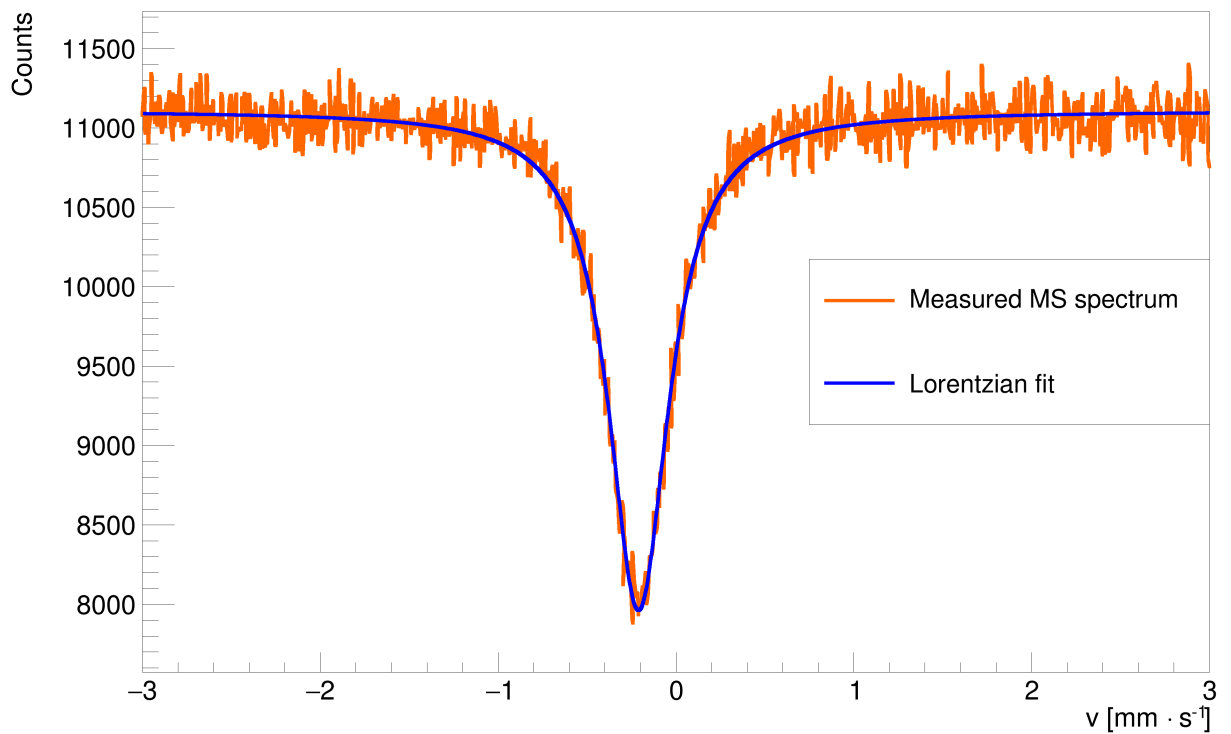


Figure 10.2: Gas detector  $\text{K}_3[\text{Fe}(\text{CN})_6]$  MS spectra.

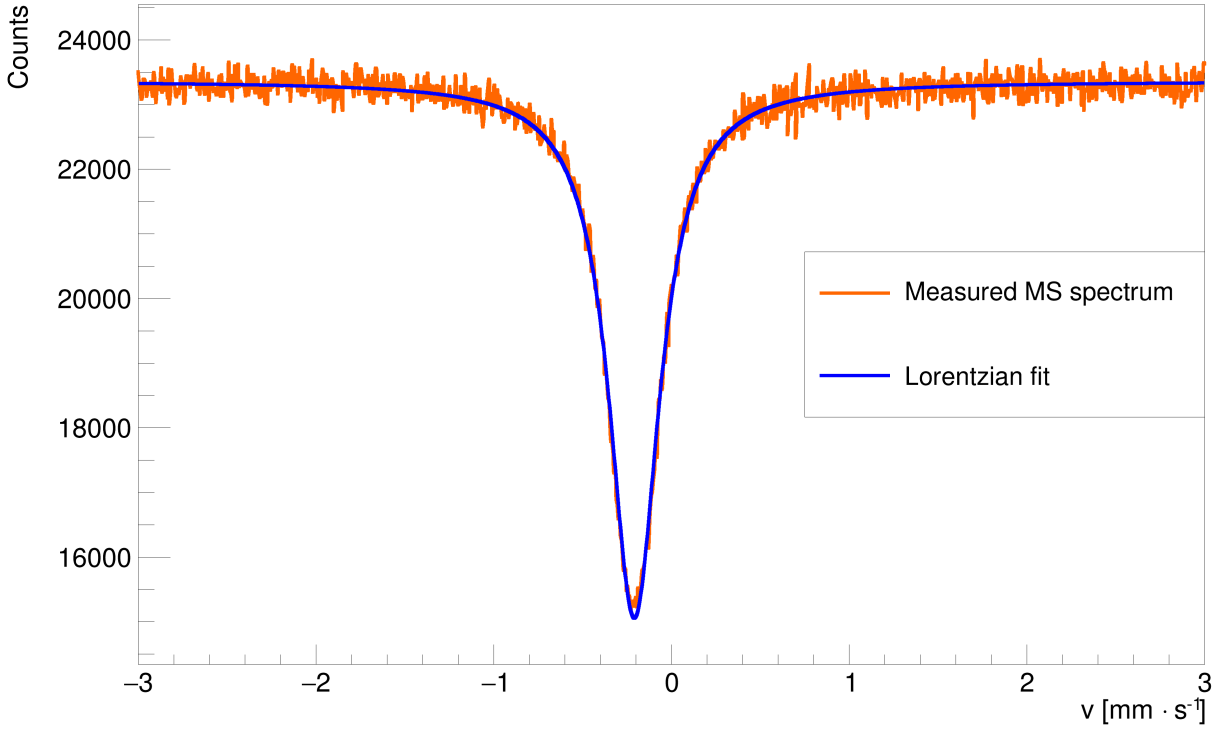


Figure 10.3: Scintillator detector  $\text{K}_3[\text{Fe}(\text{CN})_6]$  MS spectra.

Every spectra is fitted by the Lorentzian in the form described by equation 4.1. However, in order to compare the MS parameters between detectors, there was a problem with the different  $\Gamma$  in every spectra, which is not caused by the detector, but probably by the transducer. If the  $\text{SNR}_{\text{MS}}$  and  $E_{\text{MS}}$  (equations 4.3 and 4.4), which both depend on  $I$ , are to be comparable between the measurements, it is necessary to recalculate the  $I$  for every Lorentzian. The recalculation is based on the following consideration: The altered velocity signal can cause the variations in  $\Gamma$  of a singlet Lorentzian curve, however, its area  $A$  (total number of counts) given by equation 4.2 should be left unchanged by this effect. So if the  $A$  is conserved although the  $\Gamma$  is changed, the new amplitudes  $I_{\text{rec}}$  corresponding to the recalculated Lorentzians with the same  $\Gamma_{\text{ref}}$  can be obtained by a simple relation  $I_{\text{rec}} = \frac{\Gamma}{\Gamma_{\text{ref}}} I$ . As a reference  $\Gamma_{\text{ref}}$  is taken the smallest  $\Gamma$  of the three detectors. The results obtained for every detector can be seen in table 10.1.

	$\text{SNR}_{\text{MS}}$	$E_{\text{MS}}$
Si PIN	$27.4 \pm 0.5$	$0.444 \pm 0.007$
gas	$35.7 \pm 0.5$	$0.338 \pm 0.005$
scintillator	$54.3 \pm 0.3$	$0.355 \pm 0.002$

Table 10.1: Measured  $\text{SNR}_{\text{MS}}$  and  $E_{\text{MS}}$  for every detector.

The results show that the best  $\text{SNR}_{\text{MS}}$  has the scintillator detector, and thus when it comes to acquiring the MS spectra in transmission geometry, the Si PIN detector is not the best candidate. However, the highest  $E_{\text{MS}}$  is associated with the Si PIN, and thus it can be employed in some applications where  $E_{\text{MS}}$  is an important parameter.

# Conclusion

The first tests of Si PIN photodiodes were performed on setup consisting of ORTEC modular parts. All the three selected photodiodes (S14605, BPW34 and OPF430) produced spectrometric pulses and the gamma spectra of  $^{57}\text{Co}$  were successfully measured and interpreted. Characteristic full energy peaks of  $^{57}\text{Co}$  (14.4 keV, 122.1 keV and 136.5 keV) were observed as well as expected Compton continuum originating from Compton scattering of 122.1 keV inside the detector. It was found out, that the electromagnetic shielding plays a very important role in noise reduction. The Si PIN photodiodes attached to charge preamplifier can not work properly without sufficient shielding. Cooling the photodiode also had an effect, but its significance was much lower.

It was proven, that even a cheap Si PIN photodiode (BPW34 and OPF430) originally intended for detection of light can be employed as detector for gamma spectroscopy. However, it was shown that their detection efficiency is much worse than the detection efficiency of photodiode S14605, which is classified as x-ray detector.

The front-end analog electronics for Si PIN detectors in form of PCB consisting of Crema modules and SMD parts was successfully developed. This designed PCB placed into the shielding box integrates a significant part of spectrometric chain inside itself - PIN photodiode, the charge preamplifier, two amplification stages, the shaper and the high voltage supply for photodiode in form of a charge pump. For its functionality it requires only +15 V and -15 V power supply. Its output can be directly routed to the MCA. This Si PIN detector with integrated amplifier Int a full observation of 14.4 keV energy peak. The MS measurement setup employing constructed Si PIN detector was successfully assembled and the transmission MS spectra of a singlet sample was successfully measured.

Two types of measurements were performed in order to compare the Si PIN detector with gaseous and scintillator detector - the measurement of 14.4 keV realative detection efficiency and the MS measurement. The only parameter of the Si PIN detector, which can be characterized as the best among the tested detectors is  $E_{\text{MS}}$ .

The development of PIN detector for transmission MS spectroscopy can continue by employing the photodiodes with better detection efficiency - by using Si photodiode with greater thickness or by using a photodiode made of a different material with higher  $Z$  (for example Ge). To fully observe 6.4 keV energy peak, it will be necessary to employ a photodiode with lesser capacitance (greater thickness also implies lesser capacitance) or a preamplifier with a better characteristics. The development can also go on by the mathematical modelling of a better semiconductor detector for MS and by a theoretical simulations of its detection efficiency by using some of well-known programs for the simulation of passage of particles through matter such as the Geant4 [16].

The work on thesis was both very hard and experiencing, and thus it can be compared to have to chug a bottle of 50% vodka - get sick, get experienced.

# Bibliography

1. NOVÁK, Petr. *Mössbauerův spektrometr s časovým rozlišením detekce fotonů záření gama - vývoj a aplikace [online]*. 2016 [cit. 2023-11-06]. Doctoral theses, Dissertations. Palacký University Olomouc, Faculty of ScienceOlomouc.
2. STEJSKAL, Aleš. *Konstrukce duálního Mössbauerova spektrometru a adaptace pro dynamická měření [online]*. 2019 [cit. 2023-11-06]. Master's thesis. Palacký University Olomouc, Faculty of ScienceOlomouc.
3. MARISCOTTI, M.A. A method for automatic identification of peaks in the presence of background and its application to spectrum analysis. *Nuclear Instruments and Methods*. 1967, vol. 50, no. 2, pp. 309–320. ISSN 0029-554X. Available from DOI: [https://doi.org/10.1016/0029-554X\(67\)90058-4](https://doi.org/10.1016/0029-554X(67)90058-4).
4. LEO, William R. *Techniques for nuclear and particle physics experiments: A how to approach*. Berlin: Springer-Verlag, 1987. ISBN 9783540572800.
5. RAMIREZ-JIMENEZ, F.J.; LOPEZ-CALLEJAS, R.; CERDEIRA-ALTUZARRA, A.; BENITEZ-READ, J.S.; ESTRADA-CUETO, M.; PACHECO-SOTELO, J.O. PIN diode-preamplifier set for the measurement of low-energy gamma and X-rays. *Nuclear Instruments and Methods in Physics Research Section A: Accelerators, Spectrometers, Detectors and Associated Equipment*. 2003, vol. 497, no. 2, pp. 577–583. ISSN 0168-9002. Available from DOI: [https://doi.org/10.1016/S0168-9002\(02\)01806-5](https://doi.org/10.1016/S0168-9002(02)01806-5).
6. LUTZ, Gerhard. *Semiconductor radiation detectors: Device physics*. Berlin: Springer, 2007. ISBN 9783540716785.
7. GILMORE, Gordon. *Practical gamma-ray spectroscopy*. 2nd ed. Chichester u.a.: Wiley-Blackwell, 2008. ISBN 9780470861967.
8. PROCHÁZKA, Vít. *Neobvyklá Mössbauerova spektroskopie*. Olomouc: Palacký University Olomouc, 2014. ISBN 9788024440118.
9. HILL, Paul Horowitz; WINFIELD. *The Art of Electronics, 3rd Edition*. Cambridge: Cambridge University Press, 2015. ISBN 0521809266.
10. KOURIL, Lukas; PECHOUSEK, Jiri; KOHOUT, Pavel; JIRUŠ, Marek; SCHLAT-TAUER, Leo. *Optimized conversion X-rays Mössbauer setup for efficient bulk sample surface analysis*. 2021.
11. AMPTEK. *Si-PIN vs CdTe Comparison*. Available also from: <https://www.amptek.com/internal-products/si-pin-vs-cdte-comparison>.
12. AUTODESK. *Autodesk Eagle*. Available also from: <https://www.autodesk.com/products/eagle/overview?term=1-YEAR&tab=subscription>.
13. BECQUEREL, Laboratoire National Henri. *Co-57*. Available also from: [http://www.lnhb.fr/nuclides/Co-57\\_tables.pdf](http://www.lnhb.fr/nuclides/Co-57_tables.pdf).

14. *CERN DIY Particle Detector* [online] [visited on 2023-12-26]. Available from: <https://physicsopenlab.org/2020/06/15/cern-diy-particle-detector/>.
15. ELECTRONICS, TT. *OPF430* [online] [visited on 2023-12-26]. Available from: <https://cz.mouser.com/datasheet/2/414/OPF430-3241495.pdf>.
16. GEANT4. *Geant4, a toolkit for the simulation of the passage of particles through matter*. Available also from: <https://geant4.web.cern.ch/>.
17. HAMAMATSU. *S14605* [online] [visited on 2023-12-26]. Available from: [https://www.hamamatsu.com/content/dam/hamamatsu-photonics/sites/documents/99\\_SALES\\_LIBRARY/ssd/s14605\\_kpin1091e.pdf](https://www.hamamatsu.com/content/dam/hamamatsu-photonics/sites/documents/99_SALES_LIBRARY/ssd/s14605_kpin1091e.pdf).
18. HAMAMATSU. *Si detectors for high energy particles* [online] [visited on 2023-12-26]. Available from: [https://www.hamamatsu.com/content/dam/hamamatsu-photonics/sites/documents/99\\_SALES\\_LIBRARY/ssd/high\\_energy\\_kspd9002e.pdf](https://www.hamamatsu.com/content/dam/hamamatsu-photonics/sites/documents/99_SALES_LIBRARY/ssd/high_energy_kspd9002e.pdf).
19. HAMAMATSU. *Characteristics and use of Charge amplifier*. Available also from: [https://www.hamamatsu.com/content/dam/hamamatsu-photonics/sites/documents/99\\_SALES\\_LIBRARY/ssd/charge\\_amp\\_kacc9001e.pdf](https://www.hamamatsu.com/content/dam/hamamatsu-photonics/sites/documents/99_SALES_LIBRARY/ssd/charge_amp_kacc9001e.pdf).
20. HAMAMATSU. *HIGH VOLTAGE POWER SUPPLY SOCKET ASSEMBLY (DP-TYPE) C9028-01*. Available also from: <https://www.digchip.com/datasheets/parts/datasheet/190/C9028-01-pdf.php>.
21. HAMAMATSU. *Photomultiplier tubes R6094, R6095*. Available also from: [https://www.hamamatsu.com/content/dam/hamamatsu-photonics/sites/documents/99\\_SALES\\_LIBRARY/etd/R6094\\_R6095 TPMH1382E.pdf](https://www.hamamatsu.com/content/dam/hamamatsu-photonics/sites/documents/99_SALES_LIBRARY/etd/R6094_R6095 TPMH1382E.pdf).
22. INC, Cremat. *Advice in using Cremat CSP modules* [online] [visited on 2023-12-26]. Available from: <https://www.cremat.com/applications/csp-application-notes/>.
23. INC, Cremat. *CR-110-R2 charge sensitive preamplifier* [online] [visited on 2023-12-26]. Available from: <https://www.cremat.com/CR-110-R2.pdf>.
24. INC, Cremat. *CR-200 Gaussian shaping amplifier* [online] [visited on 2023-12-26]. Available from: <https://www.cremat.com/CR-200-R2.1.pdf>.
25. INSTRUMENTS, Texas. *Grounding in mixed-signal systems demystified, Part 1*. Available also from: <https://www.ti.com/lit/an/slyt499/slyt499.pdf>.
26. INSTRUMENTS, Texas. *OPA847*. Available also from: <https://www.ti.com/lit/ds/symlink/opa847.pdf>.
27. KLINGELHÖFER, G. et al. Athena MIMOS II Mössbauer spectrometer investigation. *Journal of Geophysical Research: Planets*. Vol. 108, no. E12. Available from DOI: <https://doi.org/10.1029/2003JE002138>.
28. NIST. *Atomic Weights and Isotopic Compositions for All Elements*. Available also from: [https://physics.nist.gov/cgi-bin/Compositions/stand\\_alone.pl](https://physics.nist.gov/cgi-bin/Compositions/stand_alone.pl).
29. ORTEC. *EASY-MCA-8K EASY-MCA-2K Digital Gamma-Ray Spectrometer User's Manual*. Available also from: <https://www.ortec-online.com/-/media/ametekortec/manuals/e/easy-mca-mnl.pdf>.
30. ORTEC. *Introduction to Amplifiers*. Available also from: <https://www.ortec-online.com/-/media/ametekortec/other/amplifier-introduction.pdf>.

31. ORTEC. *MAESTRO Multichannel Analyzer Emulation Software*. Available also from: <https://www.ortec-online.com/products/software/maestro-mca>.
32. ORTEC. *Models 142A, 142B, and 142C Preamplifiers Operating and Service Manual*. Available also from: <https://www.ortec-online.com/-/media/ametekortec/manuals/1/142abc-mnl.pdf>.
33. SEMICONDUCTORS, Vishay. *BPW34, BPW34S* [online] [visited on 2023-12-26]. Available from: <https://www.vishay.com/docs/81521/bpw34.pdf>.
34. SPIELER, Helmuth. *Front-End Electronics and Signal Processing* [online] [visited on 2023-12-26]. Available from: [https://www-physics.lbl.gov/~spieler/ICFA\\_Morelia/text/Front\\_End\\_Electronics\\_old.pdf](https://www-physics.lbl.gov/~spieler/ICFA_Morelia/text/Front_End_Electronics_old.pdf).